university of groningen

ASTRON

MASTER RESEARCH PROJECT

Radio continuum in HI-selected galaxies from the Apertif surveys

Student: Giuseppe Ussia

Supervisor: Dr.Betsey Adams

Abstract

I present a comparative analysis of star formation rate (SFR) tracers, at different electromagnetic bands, in a sample of HI-selected galaxies taken from Apertif HI survey. In addition to the presence of atomic gas, I require them to also have a radio continuum (RC) counterpart, performing a cross match with the Apertif DR1 catalog. I get their corresponding infrared (IR) data from WISE survey and I later use information with improved extended source photometry (T. Jarrett, priv. comm.). The purpose of this study is to explore the consistency of SF tracers at different bands, test the far-IR-Radio correlation and see how well radio continuum works as a SF tracer in dwarf galaxy regimes. I performed a visual inspection procedure, aimed at identifying possible AGN contaminations that often occur in the radio band. As a result, I created a subsample of galaxies having a good match of RC contours with the shape of the source as seen in WISE W1 photometry. Then, I investigated the relations of SFRs at different IR bands with the RC based one. Finally, I performed a further comparison with the far-ultraviolet (FUV) SFR tracer derived from GALEX data. The trends between the WISE W3 ($12\mu m$) and W4 ($22\mu m$) band derived SFRs and the RC SFRs are relatively tight linear relations. However, when using the mid-IR SF tracer, derived from a combination of W3 and W4, including a correction calibrated from galaxies with FUV data to account for the typical low dust content of smaller galaxies, the IR SFR vs RC SFR trend clearly deviates from a one-to-one line, with a discrepancy at small values. The final FUV test has not confirmed the reliability of the RC or IR tracers at lower SFR values. Therefore, further investigations are advisable, for example using improved Apertif data products and a more dwarf-dominated sample.

Table of Contents

Acknowledgements

I would like to thank my supervisor, Dr. Betsey Adams, for guiding me through the project and for her invaluable advice on the research subject as well as on the general approach to the analysis. From this collaboration, I learn not only science but also scientific method.

I am deeply grateful to Prof. Thomas Jarrett who kindly provided me with data and information that were essential to my study.

I also want to express my sincere appreciation to scientists from ASTRON who have contributed to my work sharing new data and suggestions.

I would like to thank Kim W. who has always supported me along the way.

CHAPTER 1: INTRODUCTION

1.1 GALAXIES

Galaxies are cosmic objects, each containing dark matter, gas, dust and millions or billions of stars, bound together by gravity. Nowadays, we know that the Universe is filled with more than two trillion galaxies out to very large distances (Conselice et al. 2016). The astronomer Edwin Hubble, back in 1926, set up a system to classify galaxies according to their morphologies (Hubble E.P. 1926); this classification is still used at present days with some modifications and additions. The three main categories in the Hubble system (Figure 1) are:

- **Elliptical galaxies**, relatively featureless and spherical. These are indicated with the letter "*E*" and they are divided into subclasses based on how round they appear.

- **Spiral Galaxies**, with very distinctive arms out from their centers. These are distributed into two subclasses, regular spirals (S) and barred spirals (SB), the latter includes our Milky Way. Both regular and barred spirals have a spherical bulge of stars at their centers is surrounded by a thin rotating disk of stars that contains many spiral arms. The two main subclasses of spirals are further divided into sub-categories depending on how prominent the spiral arms appear.

  Lenticular galaxies appear to be an intermediate class between most flattened ellipticals and the most tightly compact spirals. They show clear signs of a disk and a central bulge but they have no spiral arms and little interstellar gas.

- **Irregular galaxies** are all the ones that do not fit the other two main classes. These present mixed features of ellipticals and spirals with no clear structures and shapes. These are mostly star forming galaxies.

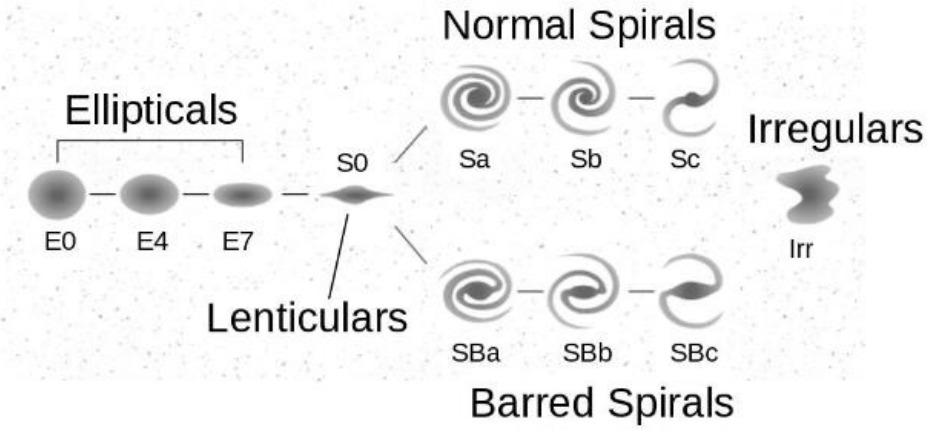

Figure 1: The Hubble classification schema for galaxies

There is a correlation between the physical differences of galaxies and the different Hubble types (Kennicutt 1998). One such property is the angular momentum, related to the rate at which the various parts of the galaxy rotate about the centre, and its degree of compactness. Overall, the angular momentum per unit mass of elliptical and irregular galaxies is low, whereas it is relatively high for spirals and lenticulars (Ogle P.M. et al. 2019).

Another property correlated with Hubble class concerns the ratio of the mass gas to the total mass of stars in a galaxy. And specifically, the presence of molecular or atomic gas determines other important characteristics such as the mass, luminosity and size of galaxies. This is because there is a linear proportionality between the surface density of the star formation rate (SFR) with the surface density of molecular hydrogen (Schruba et al. 2010).

Ellipticals contain many old stars and a very little gas between them; thus, they lack the raw ingredients to make new luminous stars and consequently they do not look as bright as other galaxy types per unit stellar mass. Ellipticals are therefore called *dying galaxies* and they are the most commonly observed. Their masses vary from 10^9 to over 10^{13} $\mathrm{M}_\odot$ (Longair 2007).

Spiral galaxies have a mix of young and old stars as there is a significant amount of gas and dust that fill the disk; thus in the disk new star formation takes place continuously (Salim S. et al. 2007). Spirals have a narrow range of masses, from 10^9 to a few times 10^{12} $\mathrm{M}_\odot$.

Whereas irregular galaxies are simply more chaotic, they can be very bright and host many young stars. They exhibit an intermediate range of properties, with masses from 10^7 to 10^{10} $\mathrm{M}_\odot$.

Galaxies do not appear the same way they formed. They can change over cosmic time as a result of interactions, collisions and mergers between them (Hernquist 1995). Such interactions of galaxies trigger bursts of star formation and change their own characteristics in a process known as galaxy evolution.

1.1.1. GALAXY FORMATION IN A NUTSHELL

To the best of our knowledge, galaxy formation begins when dark matter merges and assembles in small objects, called dark matter halos, that later, grow up to build larger halos in a hierarchical way. As these structures expand with time, the present gas and dust components start to create luminous stars. The latter evolve and die cyclically to form new star generations (Cattaneo A. et al. 2011), bound into larger systems: galaxies.

Also galaxies are thought to grow up hierarchically: scientists have proved that most of earlier galaxies tend to be smaller and more irregular than the present-day ones (Cole S. et al. 2000). However, this is not univocal, as some distant galaxies appear similar to the ones nearby.

1.2 DWARF GALAXIES

Dwarf galaxies constitute the largest subset of galaxies in the Universe (Cross et al. 2004); they have a great cosmological importance as considered to have been the first to form and then merged, in hierarchical scenarios, to create bigger galaxies. Dwarfs are metal-poor systems thus, very appealing to astronomers as assumed to be highly unevolved and excellent laboratories to study primordial conditions (Tolstoy et al. 2009). However, they are not well understood as small and faint. They may also contain a larger amount of dark matter than of luminous masses (Lee J et al. 2009). These "tiny" systems have low masses ($M \leq 10^9\ M_\odot$), low metallicity ([Fe/H] < -3) (Simon J.D. 2019) and relatively low luminosity (~ $10^9\ L_\odot$).
Like normal galaxies, also dwarfs can be classified into subclasses; the two main ones are:

- Late-type galaxies, star forming systems → dwarf irregular galaxies (dIs) and blue compact dwarf (BCD) galaxies;

- Early-type systems, not currently forming stars → dwarf ellipticals (dEs) and dwarf spheroidals (dSphs) with the recent addition of ultra-faint dwarf galaxies that are mostly like dSphs, but noted for their extremely faint luminosities.

DIs are particularly interesting because they are characterized by recent star formation. They have irregular visual appearance, large HI (atomic hydrogen) gas reservoirs (Hoffman G. et al. 1996) and low dust content (Calzetti 2001). Their morphology is chaotic with a lack of spiral structures and active star formation across the whole galaxy (Hunter 1997). DIs and BCDs are very similar but the latter have a higher star formation rate (Papaderos et al. 1994). Whereas, dwarf ellipticals (dEs) and dwarf spheroidals (dSphs) mostly contain old stars, and low gas content, therefore not ongoing or recent star formation (Ferguson & Binggeli 1994). These two subclasses slightly differ in mass (Han et al. 1998).

1.3 STAR FORMATION

Stars form in dense interstellar clouds, composed of molecular hydrogen (H_2). The process begins when the gas cools down under $100\ \mathrm{Kelvin}$ and consequently undergoes a gravitational collapse turning into stellar mass. H_2 is particularly efficient in forming stars as it can cool down significantly: its roto-vibrational transitions cause energy loss thus, gas cooling (Longair 2007). The dust component of galaxies, mostly provided by supernovae explosions, is a crucial player in the star formation (SF) processes as it helps H_2 to form on dust grains (Calzetti 2007). Furthermore, dust is responsible for the absorption and reprocessing of the ultraviolet (UV) and visible light, emitted by the newborn massive stars, into the infrared (IR) range. This last concept will be further analyzed in the next subsection.

Measuring the rate at which a galaxy forms its stellar mass - the star formation rate SFR - is essential to know the physical processes in galaxy evolution; therefore, it is a distinctive property of different galaxy types. SFRs are measured in units of $M_\odot/\mathrm{yr}$. When stars form, depending on their intrinsic characteristics (mass, temperature and size), they can emit radiation at different wavelengths; therefore, SF processes can be traced using different indicators (Kennicutt et al. 2009; Calzetti 2012). The basic idea behind the SFR measurement is to analyse the galaxy fluxes, at specific wavelengths, in a way to disentangle the stellar

continuum or the emission line of recently formed stars from the contributions of older stellar populations (Calzetti et al. 2007). More massive stars, O and B, burn their fuel at a higher speed, hence they have a shorter lifetime ($\leq 3 \times 10^7\ yrs$). For this reason they are the most studied to measure the galaxy SFR as they simply formed "more recently" with respect to the others, tracing a recent SF activity.

A key ingredient in SF activity is the initial mass function IMF as it specifies the number of stars in a certain mass range for a freshly formed stellar population (Carigi 2011). Therefore, the IMF gives clues on how many massive young stars form in a specific event. The IMF is a mathematical expression; the most popular is the form of a power law (Salpeter 1955) or a combination of power laws (Kroupa et al. 1993) that describes the mass-spectrum of stars born collectively in "one event".

1.4 STAR FORMATION TRACERS

Galaxies can be very diverse in forms and shapes as well as stellar populations, star forming activity and interstellar medium (ISM) properties. Therefore, their SFR can be traced using different indicators.

The Hα emission line and the ultraviolet (UV) flux are important SFR tracers. In particular, the first one originates from the recombination of the ionized hydrogen gas of nebular clouds by the starlight of the most massive O and B type stars ($\mathrm{M} \gtrsim 17\,\mathrm{M}_\odot$); it therefore traces star formation activity occurring over a few million years that corresponds to the lifetime of these star classes. Whereas, the UV light comes directly from the photosphere of stars in a larger mass range ($\mathrm{M} \gtrsim 3\,\mathrm{M}_\odot$) hence it traces star formation activity over loger timescales $\sim 10^8$ yr (Lee J.C. et al. 2009). However, the UV light is extincted by dust and re-emitted at infrared (IR) wavelengths (Reddy et al. 2015) while the Hα emission line is less attenued (Kewley et al. 2002).

Due to the dust extinction effects just mentioned, the IR band offers reliable tracers of SF, in relation to the dust content in galaxies and the dust opacity. It is important to mention that both massive short-lived stars and low-mass, long-lived stars can heat the dust. In particular, the galaxy luminosity at mid/far-IR (MIR, FIR) wavelengths (~ *5-1000 μm*), indicated as L_{TIR}, probes the dust heated by young (*1-100 Myrs*) UV luminous O and B stars as well as intermediate mass stars.

In addition, SFR can be also traced from radio continuum (RC) emission (Condon 1992). There are two different components of radio luminosity in a galaxy. One is given by the thermal bremsstrahlung from ionized hydrogen in HII regions, which directly tracks forming stars as the amount of ionized hydrogen reflects the ionizing luminosity of the very young stellar populations. The second component is the non-thermal synchrotron emission from cosmic ray electrons (CRe) spiraling in the galactic magnetic field (Condon 1992). In principle, at the end stage of their lifetime, massive stars produce Type II supernovae whose remnants (SNRs) are responsible for accelerating relativistic electrons in galaxies. Since these very massive stars have a short duration, also their relativistic electrons live for a relatively small period of time ($< 10^8 yrs$) thus, they can trace a recent SF activity (Vollmer B. et al. 2022). A good advantage of using RC emission as a SFR indicator is that radio observations are not affected by the light of older stellar populations nor by dust. However, a big limitation of RC SFR tracers is the interference from the bright

radio luminosity of active galactic nuclei (AGNs) or Type Ia supernovae that come from long lived stars (Radcliffe J.F. et al. 2021).

In order to test the reliability of individual SFR tracers, a widely used approach is to compare SFRs measured in multiple bands. Specifically, UV SFR tracers are crucial for galaxies with extended UV disks as well as for faint dwarf galaxies. The first case is that of galaxies forming OB stars in their outskirts, so in conditions of low SFR density wherein Hα might be an insufficient SF indicator (Lee J.C. et al. 2009). Whereas, dwarf galaxies have a small dust content thus a lack of extinction effects, which translates in an expected better accuracy of the UV flux than the IR luminosity as a SF tracer.

1.5 RADIO CONTINUUM – INFRARED CORRELATION

Massive stars are responsible for most of the far-infrared (FIR) luminosity of a galaxy, attributed to the dust extinction of their emitted UV-visible light, and they also produce most of the RC emission, as the SNRs cause synchrotron radiation. Therefore, the recent SF activity is well traced in these bands and a tight, ubiquitous correlation was found between the global FIR (predominantly non-thermal) and the radio luminosity of normal galaxies (Figure 2) (Condon 1992). Low massive galaxies or those with low SFRs may suffer from deviations from this correlation (Helou et al. 1985).

The slope of this correlation depends on different factors, including the galaxy IR luminosity, the frequency range and the non-thermal to thermal radio emission (Bell E.F. 2003). Samples dominated by faint galaxies ($L_{IR} < 10^{10}\ L_{\odot}$) tend to have steep radio - IR correlations; instead, for highly luminous galaxies ($L_{IR} > 10^{10}\ L_{\odot}$) the slopes are close to unity (Yun et al. 2001). This has been interpreted as in low luminous galaxies there is a larger contribution of old stellar populations heating dust to IR luminosity. Also, at low radio frequencies (< 5 GHz) the radio - IR slope is steeper than at higher frequencies due to a higher synchrotron fraction of the radio emission (Price & Duric 1992). Furthermore, the thermal radio continuum, directly tracing SF activity, correlates linearly with the IR luminosity whereas, non-thermal radio emission nonlinearly relates to SF (Bell E.F. 2003).

However, according to (Bell E.F. 2003), there is another important factor that needs to be included in such a framework: the effects of dust opacity. In fact, in highly luminous galaxies the dust is optically thick to FUV light (TIR/FUV $\gg$ 1) (Buat et al. 2002), hence, the IR emission is a plausibly good tracer of ongoing star formation activities. Instead, in low-luminosity galaxies the dust is optically thin to FUV (TIR/FUV < 1), which implies that the IR emission underestimates the SFR substantially (Wang & Heckman 1996).

If the RC emission in faint galaxies is considered as a good SF tracer while IR emission is clearly not for the aforementioned reasons, then the radio-IR correlation should not be linear. However, it was still found to be more or less linear (e.g., Yun et al. 2001) implying that non-thermal radio emission in low luminosity galaxies must be suppressed. The most likely accepted explanation is that CRes escape from the galaxy due to their small sizes (Chi & Szabelski 1992).
Thus, the linearity of the radio–IR correlation is a conspiracy: both indicators underestimate the SF rate at low luminosities in coincidentally quite similar ways.

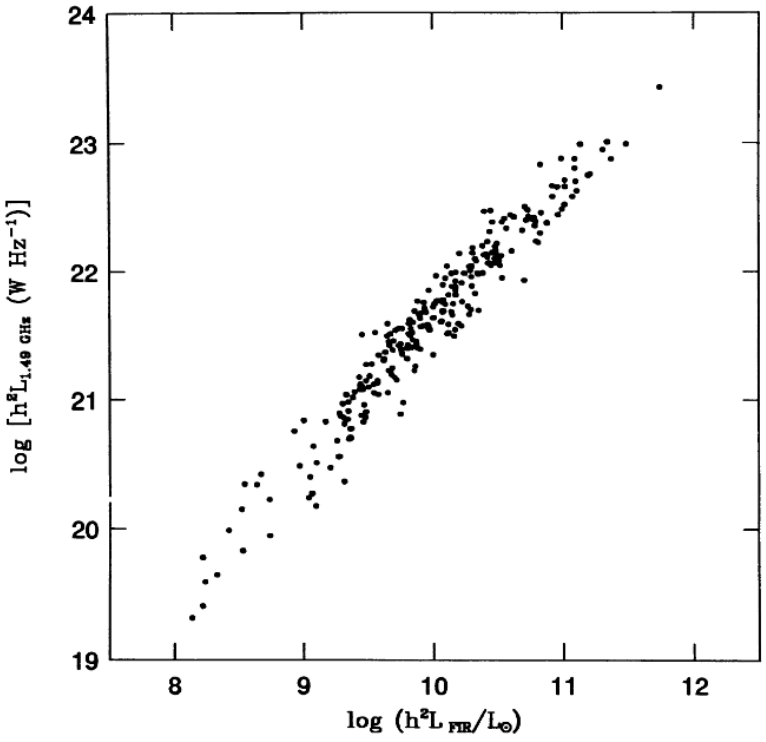

Figure 2: FIR-Radio correlation for star forming galaxies, corresponding to *Figure 8* in Condon et al. 1992. The FIR observations refer to a wavelength of $\lambda = 60\ \mu m$ whereas the radio observations to a frequency of $1.48\ GHz$.

CHAPTER 2: DATA

2.1 APERTIF

For the purpose of conducting a star formation analysis of the chosen galaxy sample, I took data provided by the state of the art new generation observing system, Apertif, installed on the Westerbork Synthesis Radio Telescope (WSRT) (Adams E.A.K. et al. 2022).

- In particular, Apertif HI survey (van Cappellen W. A. et al. 2021) provides useful information of the HI emission as well as the kinematics for nearby sources. In addition, the HI measurement also gives a redshift and hence distance to the galaxy. With an improved sensitivity, Apertif aims at characterising and better constraining gas accretion hence galaxy evolution as one of its key science cases (Adams E.A.K. et al. 2022). Another main goal of Apertif HI survey is to detect the smallest gas-rich nearby galaxies that could reveal significant clues on early galaxy formation.

  In this study, I used a HI catalog of 1235 objects produced by K. Hess (priv. comm.). This comes from 4.5 months of data (mid-August - 31 December 2019).

- Furthermore, Apertif is also designed to investigate the star formation of radio faint, nearby, galaxies. Specifically, Apertif **DR1** survey is a collection of 249,672 radio sources organised in 3074 radio continuum images, created at a central frequency of $1355\ \mathrm{MHz}$ (Kutkin A. M. et al. 2022). The radio continuum catalog covers one year of observing, 1 July 2019 - 30 June 2020; but it has a requirement on data quality so that only a fraction of images (3374) is available.

When studying SF in galaxies, usually SF indicators in different bands of the electromagnetic spectrum are compared as a test of their individual reliability. And especially, having RC data of star forming galaxies calls for their counterparts in the IR window.

2.2 WISE

The WISE angular resolution is suitable for providing a sensitive all-sky survey in the mid-infrared with a great variety of targets including brown dwarfs, ultra-luminous galaxies, nearby galaxies, AGNs, interstellar dust and young stars (and many more) (Wright et al. 2010).

The WISE telescope has a high sensitivity spectral response in four main infrared bands: W1 at $3.4\ \mu m$, W2 at $4.6\mu m$, W3 at $12\mu m$ and W4 at $22\mu m$. The two near-infrared (NIR) bands, W1 and W2, are particularly efficient to track the emission from evolved stars and the galactic interstellar medium hence, they are widely used to measure galaxy stellar masses and the mass-to-light-ratio ($^{M}/_{L}$), where M is the galaxy stellar mass while L its luminosity (Jarrett et al. 2023). Whereas, at MIR and FIR ranges, W3 captures both atomic and molecular lines and continuum emission and W4 is sensitive to the small-grain dust continuum from star formation processes (Jarrett et al. 2013). Therefore, W3 and W4 are the most appropriate to track SF activity in galaxies.

A very comprehensive catalog for the infrared photometry of galaxies is **ALLWISE** (Cutri et al. 2013). This provides information for a number of 747,634,026 sources at all WISE bands.

The **WISE Extended Source Catalogue (WXSC)** comprises more accurate measurements of fluxes for nearby galaxies, as explained in (Jarrett et al. 2019). At very low redshifts, galaxies are likely resolved at $3.4\ \mu m$, however contaminations may occur during the extraction of photometry. Therefore, an important point of improvement by WXSC is the new total flux in the W1 band (as well as other colors) as a fundamental tracer of the stellar masses. In fact, thanks to the advanced W1 luminosity and colors, more accurate stellar-mass scaling relations were derived with better than 25-30% accuracy in more massive regimes while < 40-50% for $\mathrm{M} < 10^9\ \mathrm{M}_\odot$ (Jarrett et al. 2023).

2.2.1 ALLWISE VS WXCS

In Figure 3, I show a comparison of W1 fluxes derived in the same way as the WXSC (T. Jarrett, priv. comm.) to those in ALLWISE for my galaxy sample, selected as described in subsection 3.1. Since WXSC has improved accuracy than the earlier ALLWISE, I decided to use its new optimized data for further calculations in scope for this study.

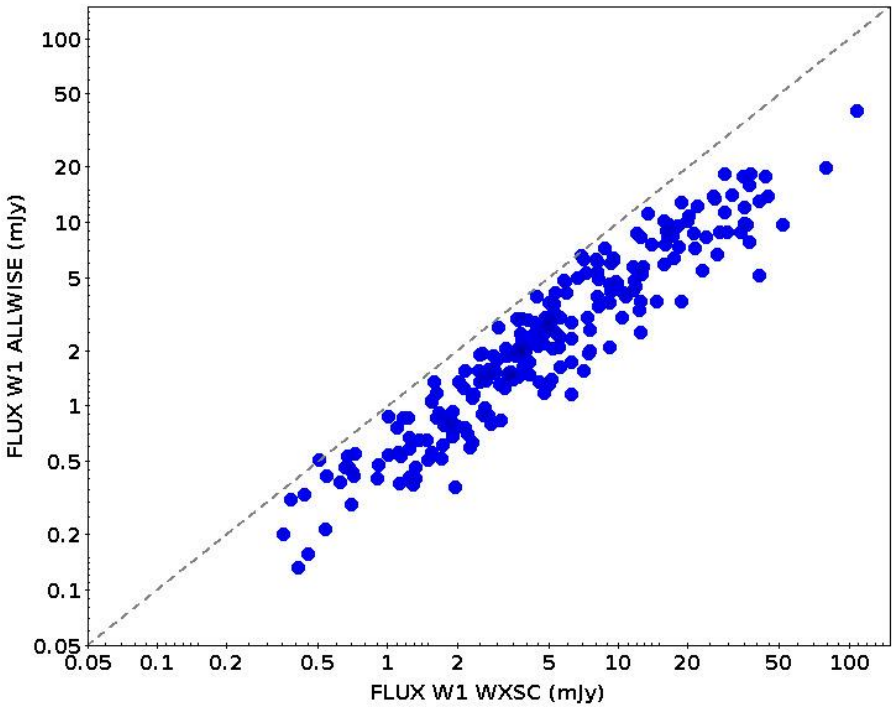

Figure 3: Comparison of W1 fluxes in WXSC and ALLWISE. The black dashed line is a one to one line for reference.

2.3 GALEX

The most direct tracer of recent SF activity comes from the young massive starlight in the UV range. In this spectral window, the Galaxy Evolution Explorer (GALEX) provides a series of sky surveys with measurements in two bands: FUV (Far Ultraviolet) with a central wavelength of $\lambda_{mean} = 1528$ Å and NUV (Near Ultraviolet) with $\lambda_{mean} = 2310$ Å (Bianchi et al. 2017).
These have really given an important contribution to the studies of hot stellar objects, star forming galaxies as well as the interstellar medium. The measured sources in the current GALEX database (data release **GR6 + 7**) are around 82,992,086 most of which well characterised in photometry at the two bands. In particular, GALEX photometry is optimised for point sources, whereas for extended sources it might result in underestimated flux densities (Burgarella et al. 2020).

CHAPTER 3: METHODOLOGY

3.1 GALAXY SAMPLE

In this section, I show how I built my galaxy sample. First, I collect all the steps in a schema then, I describe each precisely.

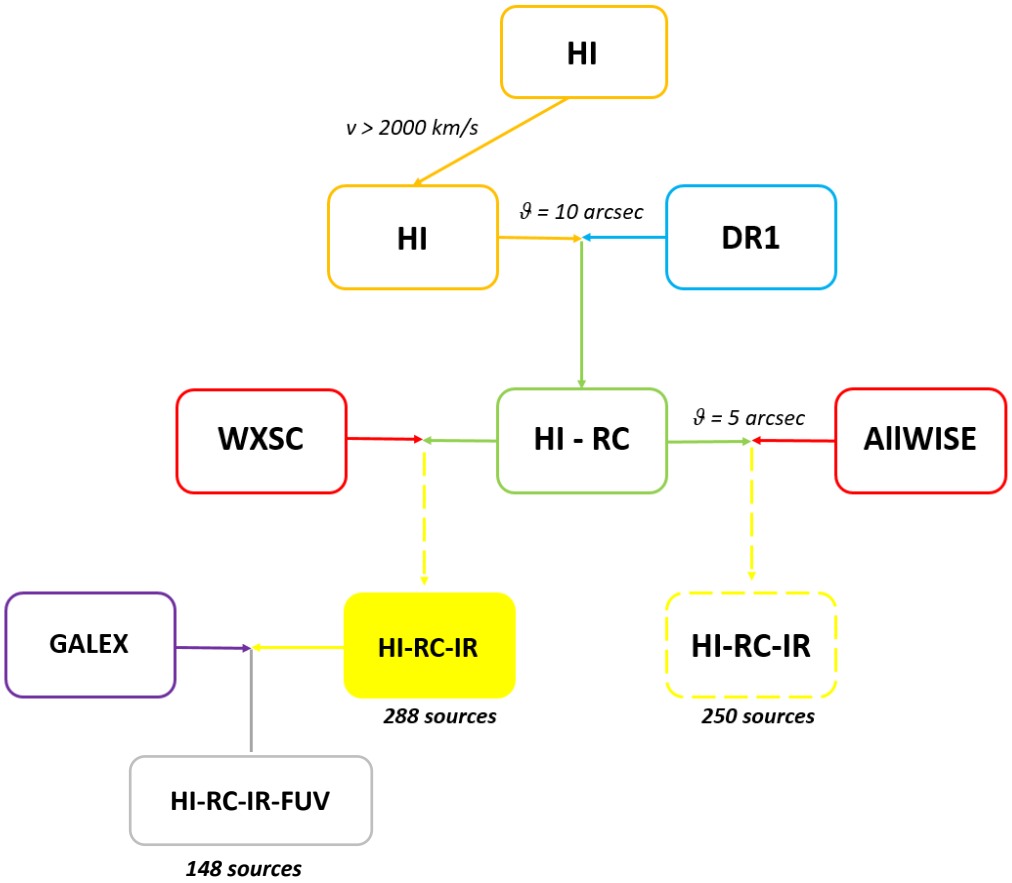

- Since I performed an analysis of star formation activity in galaxies, I needed sources with a proper gas content. This requirement is essential to find star-forming galaxies and avoid other sources i.e. AGNs. Therefore, I started from taking objects in Apertif HI catalog (K.Hess, priv. comm.) that includes data of their HI emission as well as their redshift, hence distance, crucial for the measurements of this work.
  I filtered data considering only galaxies with $v_{sys} > 2000\ km/s$ to exclude very nearby galaxies, as their peculiar motion could result in an under- or over- estimated luminosity distance, $D_L = {}^{v_{sys}}/_{H_0}$. In the end, I obtained a list of selected 1089 galaxies.

- For the purpose of studying different SFR tracers, I required these objects to also have RC emission. Therefore, I have cross-matched the selected sample of Apertif HI catalog, with Apertif DR1 catalog. In doing so, I have used an angular distance of 10 arcseconds that, from a histogram of statistics (Figure 4), has resulted in an optimal choice to include a significant number of best-matched galaxies. This cross matching has produced a sample of 288 galaxies with detected HI and RC emission. Apertif beam size is 15 arcseconds (or larger), but the centroiding accurancy can be much higher than that. However, the considered sources are extended and could have different morphologies between radio continuum and HI. Therefore, even if the centers could be known with a much higher accuracy, they could be different because galaxies have different shapes.

- Furthermore, I cross-matched the list of 288 galaxies with the ALLWISE catalog (Cutri et al. 2013). This time I used a separation of 5 arcseconds, as the resolution of WISE is much higher than Apertif's. This step produced a catalog of 250 best-matched sources with HI, RC emission by Apertif and IR data by ALLWISE. Specifically, I used this sample to compare ALLWISE with optimized IR data of the WXSC.

- T. Jarrett (priv. comm.) provided me with IR improved extended source photometry (WXSC) for all the 288 galaxies selected by cross-matching Apertif HI and DR1 catalogs.

3.1.1 FUV-IR-RC DATA

To further study the consistency of SFR tracers in the IR and radio bands, I also compared them with the FUV-derived ones. Therefore, in a later step of my analysis, I built a galaxy sample out of the cross matching between the list of 288 galaxies, described above, and *GALEX GUV_cat_AIS GR6 + 7* catalog (Bianchi 2017). I used a matching distance of 8 arcseconds that, from a histogram of statistics, has resulted in a good choice to keep a high rate of sources in the sample, 178 best - matched objects. However, 30 sources do not have FUV fluxes measured by GALEX, while the NUV are available. The FUV is considered more reliable in tracing the recent star formation, unlike the NUV wavelengths which trace a major contribution from stars with lifetimes > 100 Myrs. Therefore, in this final phase, I used a sample of 148 sources for which I had information in all the desired bands (RC, IR, FUV).

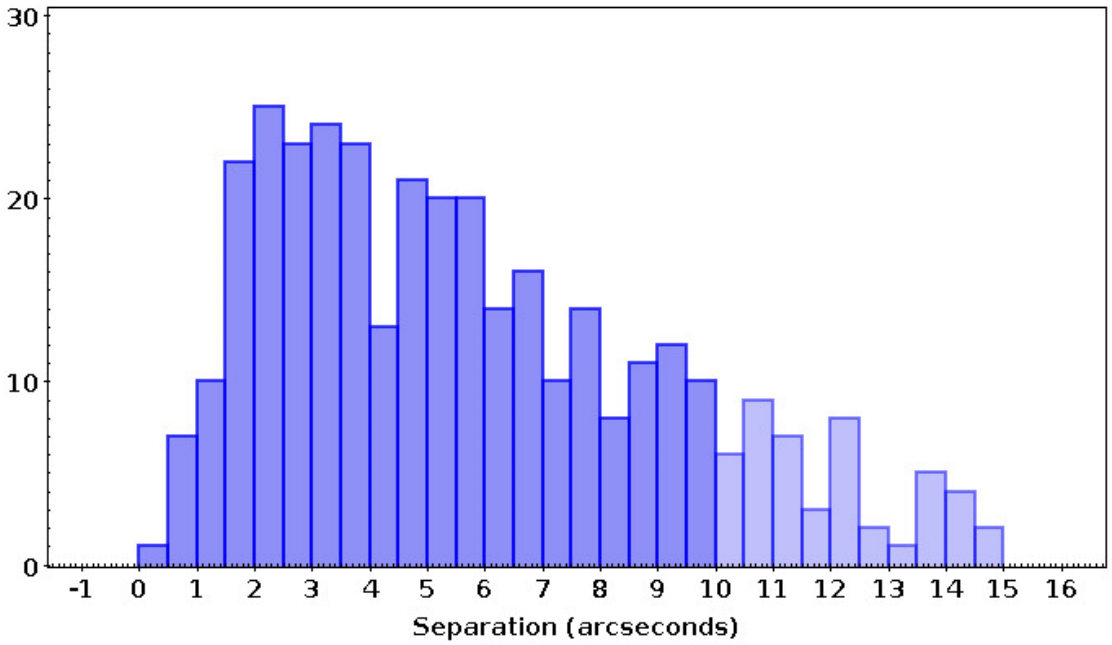

Figure 4. Histogram of statics for the choice of the tolerance (arcseconds) in cross-matching HI and DR1 Apertif catalogs. The selected tolerance is 10 arcseconds.

3.2 STAR FORMATION RATE CALCULATIONS

As a result of the available SFR tracers and the initial assumptions made (IMF, metallicity and star formation history[1]), there can be different calibrated relations to get the SFR from the galaxy luminosities at specific wavelengths. The calibration coefficients of the formulas change depending on the initial conditions (i.e. IMF and metallicity) assumed for the galaxy sample**.**

IR SFRs

One extensively used equation from the literature is connected to the L_{TIR} (Calzetti 2012), from which the SFR can be derived as:

$$SFR\left(\frac{M_{\odot}}{yr}\right) = 2.8 \times 10^{-44} \times L_{TIR}(erg\ s^{-1}) \quad (1)$$

[1] The star formation history tells how star formations occurs over time and space, whether in short bursts or over longer periods.

This expression holds for a Kroupa IMF, Starburst99 (Leitherer et al. 1999) models assuming solar metallicity and a constant star formation over *τ = 100 Myr*.
However, (Cluver et al. 2017) showed that the IR luminosity at specific bands, 12 μm and 22 μm, corresponding to W3 and W4 WISE bands, respectively, well relate to the L_{TIR} and therefore could be used as monochromatic luminosities to derive directly the SFRs (equation 4 and equation 5 in Cluver et al. 2017).

In this study, I used the IR SFRs provided in the WXSC catalog. In addition to the SFRs based on the W3 and W4 WISE band fluxes (SFR_{W3}, SFR_{W4}), there are also SFR_{mir}, derived from a combination of the two as well as a corrected value, SFR_{mircor} (Cluver et al., in preparation). The latter uses a FUV normalization that takes into account for the intrinsically lower IR SFR of low mass galaxies, as a consequence of their lower dust content compared to more massive regimes.

RADIO SFRs

A calibrated relation for RC-based SFRs is that of (Condon 2002), also followed by i.e. Heesen et al. 2014 and Cluver et al. 2017, to derive SFRs at a central wavelength of ~ 22 cm. This expression is in the form:

$$SFR_{RC}\left(\frac{\mathrm{M}_{\odot}}{\mathrm{yr}}\right) = 0.75 \times 10^{-21} \times L_{1.4GHz}(W\ Hz^{-1}) \qquad (2)$$

I employed equation (2), with radio luminosities normalized to the reference frequency of 1355 MHz, to measure the RC SFRs of my 288 galaxies.

UV SFRs

To convert the FUV fluxes I took from GALEX into UV-SFRs, I used the calibrated expression in equation 3 of (Lee C. et al, 2009) in the form:

$$SFR_{UV}\left(\frac{M_{\odot}}{yr}\right) = 1.4 \times 10^{-28} \times L_{FUV}\ \ (erg\ s^{-1}Hz^{-1}) \qquad (3)$$

As already mentioned, the FUV better traces the recent SF activity.

3.3 VISUAL INSPECTION

A crucial step I performed before analyzing the SFR trends is the visual inspection. This is because my galaxy sample might be contaminated by background sources or AGNs lying in the same field of view as well as affected by other interference (i.e. by stars....).

In this analysis, I overplotted RC contours on ALLWISE images (using the W1 band) for the 288 sources described above; some examples are presented in this subsection while all figures are shown in Appendix. I individuated four classes of objects:

1. Good data is the best collection of objects, whose RC contours perfectly follow the disk of the galaxy, which means that clearly IR and RC are tracing SF. Moreover, in this class there are also objects with RC contours concentrated in a specific part of the galaxy as I considered that SF could occur in a particular location. Some examples are shown in Figure 5. With this class of objects I produced a "clean sample" of 156 sources that I will use in my SFR trends.

2. The second class is that of objects with radio contamination from other sources, which is seen when RC contours are much bigger than the galaxy shape or when they are blended. Some examples are shown in Figure 5.

3. The third class is that of sources contaminated by others in the WISE images. To support my WISE contaminated choices I show also the corresponding images of the WXSC, provided by T. Jarrett (priv. comm.). Here contaminating sources are masked but the uncertainty still remains. Some examples are shown in Figure 6.

4. The last class contains data with a bad match of WISE and RC. The inconsistency is visible as they appear like be tracing different objects. Some examples are shown in Figure 6.

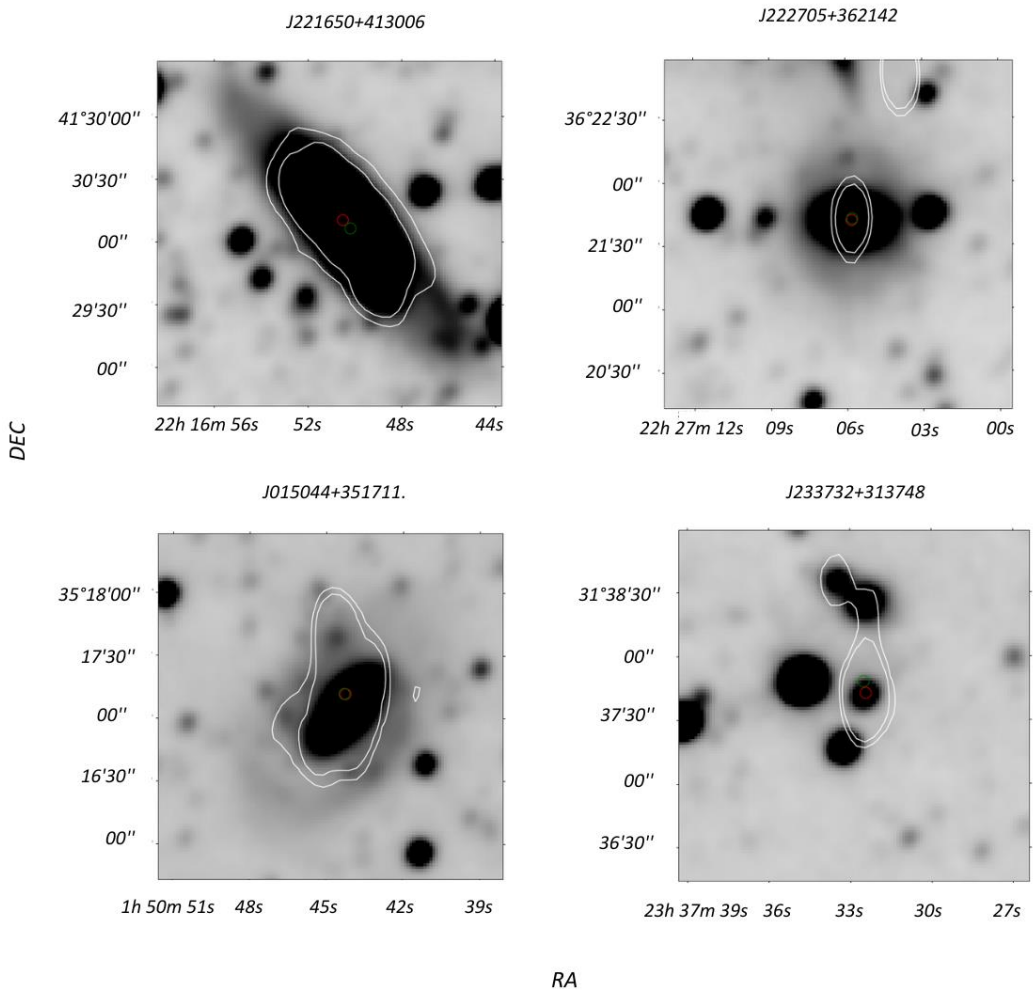

Figure 5: Top panel: two examples of good data; on the left a perfect match of radio contours with the shape of the galaxy in the WISE image whereas on the right an example of radio contours concentrated in a specific part of the galaxy. Bottom panel: two examples of radio contamination with radio contours that extend to other sources. The green and red circles are the centers of the source in WISE and RC images respectively.

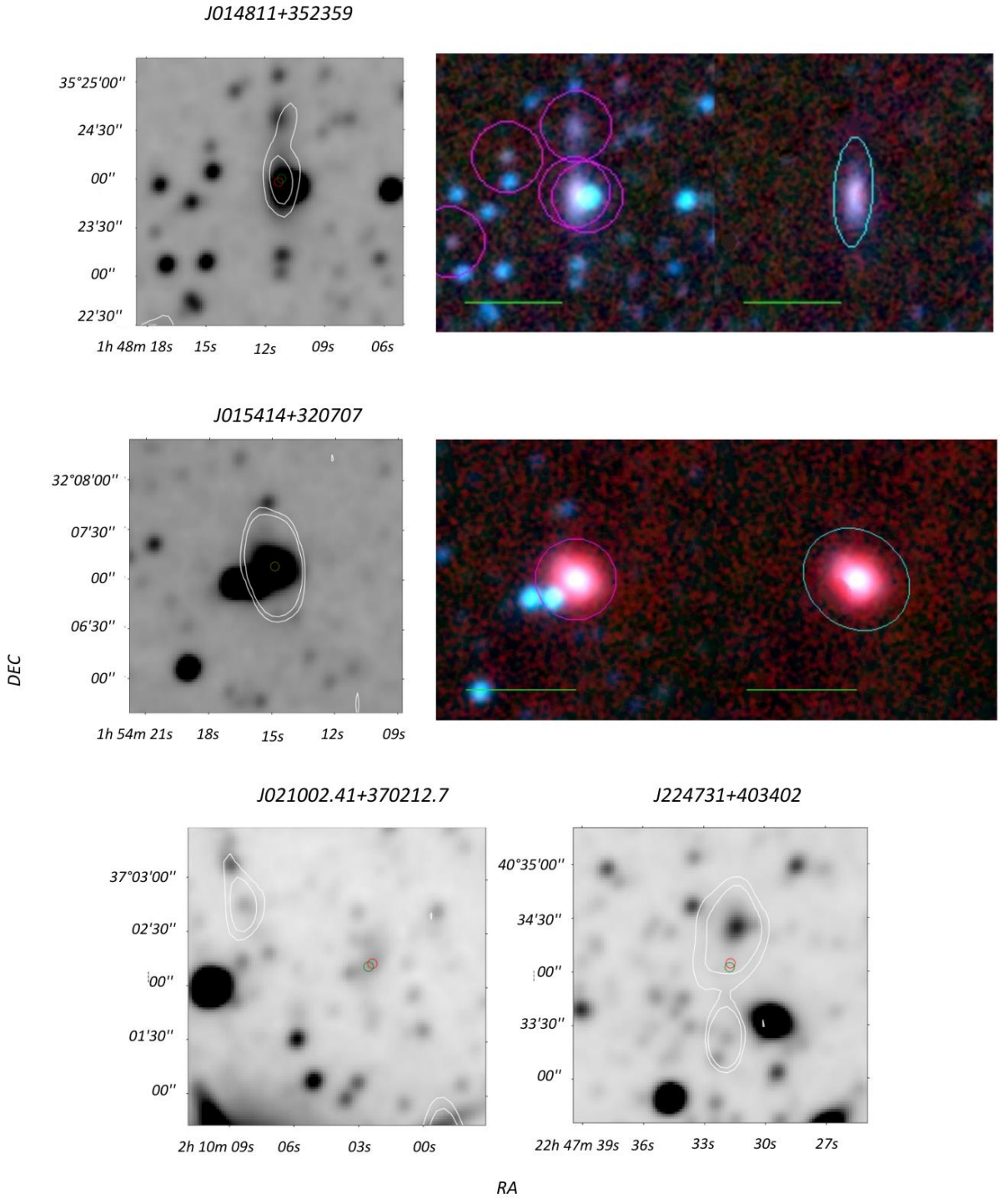

Figure 6. First two panels: examples of WISE contaminated data seen in both ALLWISE images and the corresponding images provided by T. Jarrett (priv. comm.). In the latter, contaminating sources are masked. Bottom panel: two examples of bad data where the RC and WISE do not trace a clear source and are not matched with each other. The green and red circles are the centers of the source in WISE and RC images respectively.

CHAPTER 4: RESULTS

4.1 NUMBER OF DWARF GALAXIES IN THE SAMPLE

In this step, in addition to calculating stellar masses, I explored the improvements of WXSC with respect to ALLWISE. In doing so, I compared the stellar masses of my galaxy sample, provided as WXSC data, with the ones I calculated using the W1 flux from ALLWISE.

I followed the approach described in (Jarrett et al. 2023) and reported below, to measure the stellar masses (M) of all the 250 sources of which I have ALLWISE information.

$$M_{abs} = M_{W1} - 5\,Log\left(\frac{D_L(pc)}{10}\right) \quad (4)$$

$$L_{W1} = 10^{-0.4(M_{abs}-M_{sun})} \quad (5)$$

$$Log\,M = A_0 + A_1(LogL_{W1}) + A_2(LogL_{W1})^2 + A_3(LogL_{W1})^3 \quad (6)$$

Where: $A_0 = -12.62185,\ A_1 = 5.00155,\ A_2 = -0.43857, A_3 = 0.01593$

Equation (6) shows how to estimate the stellar mass of galaxies if their infrared luminosity in the W1 band (L_{W1}) is known. The WISE W1 band, is particularly appropriate to estimate the global stellar mass of galaxies as, in that window, the luminosity is dominated by the evolved stellar populations, low mass stars that give the most significant contribution to the overall galaxy mass as they are very numerous (Jarrett et al. 2023). In equation (4) M_{abs} and M_{W1} are the absolute magnitude and the apparent magnitude in W1 band of each source, respectively, and $D_L(pc)$ the luminosity distance in parsecs. In equation (5) M_{sun} is the absolute magnitude of the Sun in the W1 band and its value is 3.24 mag (Jarrett et al. 2013).

These calculations, based on ALLWISE, have resulted in 37 found galaxies with stellar mass $\leq 10^9\ \mathrm{M}_\odot$, which I initially thought to be a fair number of dwarf galaxies (37/250) to explore. However, when improved WXSC data was available, only 9 of them survived in this low mass range, implying that ALLWISE had underestimated luminosity and thus galaxies were more massive than previously found.

4.2 STELLAR MASS VS SFR

In this section, I use the SFR derived from the WISE W3 band as well as the MIR data ($sSFR_{mir}$, $sSFR_{mircor}$) to explore their relation with the stellar masses of galaxies.

In particular, in the top panel plots of Figure 7, I compare my data to that studied by Cluver et al. 2017. Since the clean sample I am using has revealed not to include galaxies with a mass smaller than 10^9 $\mathrm{M}_\odot$, I can only test the consistency of this comparison at higher mass regimes.

In the top left plot, while the clean sample shows a more compact trend of more massive objects forming more stars, as traced in the W3 band, data points from Cluver et al. 2017 appear to have a more spread distribution with also high mass galaxies having smaller SFRs than less massive ones. Overall, there is an agreement of data in the mass range 10^9 $\mathrm{M}_\odot < \mathrm{M} < 10^{12}$ $\mathrm{M}_\odot$.

I also use the same study of Cluver et al. 2017 as a reference sample to investigate the relation between the specific SFR at W3 ($sSFR_{W3}$), which is the SFR per unit mass, and the stellar mass of galaxies. This is shown in the top right panel of Figure 7 and again there is a reasonable agreement between the two different samples in the mass range said before. However, in the sample of Cluver et al. 2017 there are more galaxies with a higher sSFR compared to those in the clean sample of this study, due to their broader mass range.

Whereas, in the bottom panel plots, I investigate the difference between the full sample and the clean sample through the relation between the $sSFR_{mir}$, & $sSFR_{mircor}$ with the stellar masses. Here a clear trend appears showing that low mass galaxies are forming relatively more stars per unit mass than the more massive ones. This is especially visible when using the corrected MIR values and it is a consequence of the FUV calibration that accounts for the lower dust content in small galaxies. This method, in fact, appears to have a significant impact only at smaller regimes.

However, the very small objects are excluded from the clean sample after the visual inspection.

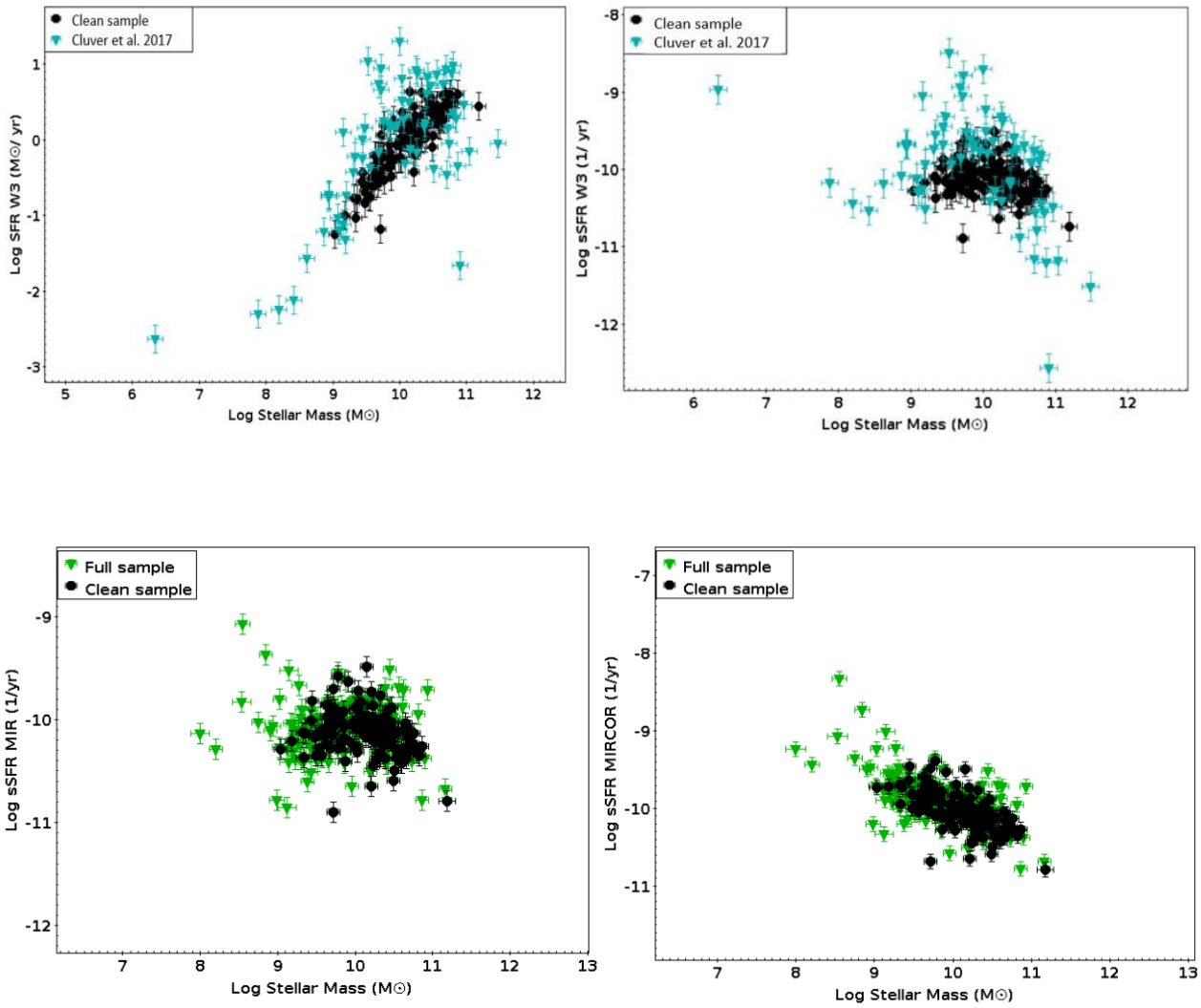

Figure 7. Top panel plots: log SFR_{W3} and log $sSFR_{W3}$ vs log stellar mass, from left to right respectively. The cyan data points correspond to the sample studied by Cluver et al. 2017. The black data points belong to the clean sample of this study. Bottom panels: the left plot shows the log $sSFR_{mir}$ vs log stellar mass while the right one the relation between the $sSFR_{mircor}$ vs log stellar mass. The black points belong to the clean sample, the green data points to the full sample.

4.3 IR vs RC SFR

Here I present the correlation between the IR derived SFRs at the WISE W3 and W4 bands with the RC based one (SFR_{RC}). I first show, in Figure 8, the three subclasses I created in the visual inspection process, the clean sample, the WISE contaminated and RC contaminated objects. The radio and WISE contaminated objects do not occupy different regions, instead, they are spread similarly all over the distribution. This suggests that radio contamination adds extra radio flux, increasing RC SFRs. On the other hand, the mask of contaminating sources in WISE images results in artificially lower measured fluxes thus lower IR SFRs.

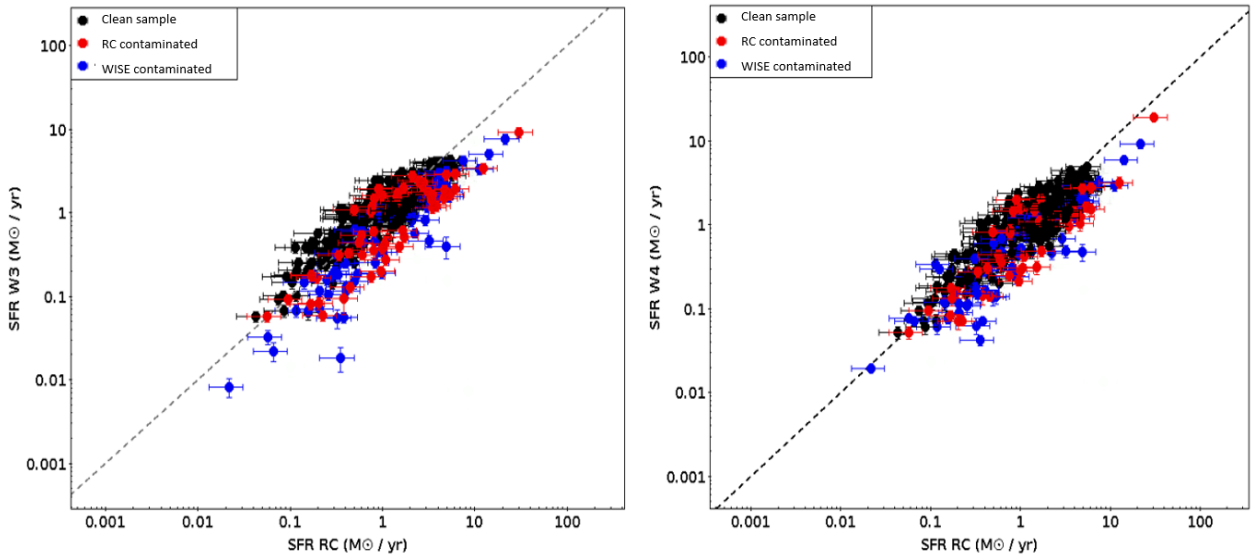

Figure 8: Plots of the SFR_{W3} vs SFR_{RC} and SFR_{W4} vs SFR_{RC} from left to right respectively. The black data points belong to the clean galaxy sample, the red ones to RC contaminations and the blue to WISE contaminations. The dashed gray line is a one to one relation for reference.

In the following plots, in Figure 9, I analyse the correlations between SFR_{W3} & SFR_{W4} with SFR_{RC} from left to right, respectively. Here, I compare the trends of the clean sample of this study with the one investigated in Cluver et al. 2017. The distributions of the two different studies look consistent. In particular, the slope of the best fit I found for SFR_{W3} vs SFR_{RC} (0.847 ± 0.015) is plausibly close to 1 and similar to that in Cluver et al. 2017 (Figure 13 a), as compared in Table 1. Data points of the clean sample are well correlated, as suggested by the Pearson correlation coefficients of 0.94, meaning that, therefore, the linear relation well describes the distribution. The estimated offset to the best fit is 0.13 consistent with that of the reference sample.

The SFR_{W4} and SFR_{RC} show an even better linear correlation of data points as suggested by the bigger Person correlation coefficient of 0.98. This linear relation has a slope of (0.881 ± 0.019), plausibly close to 1 and consistent with that of the reference sample in Cluver et al. 2017 (Figure 13 b), as compared in Table 1. The estimated offset to the best fit is 0.12, consistent with that of the reference sample.

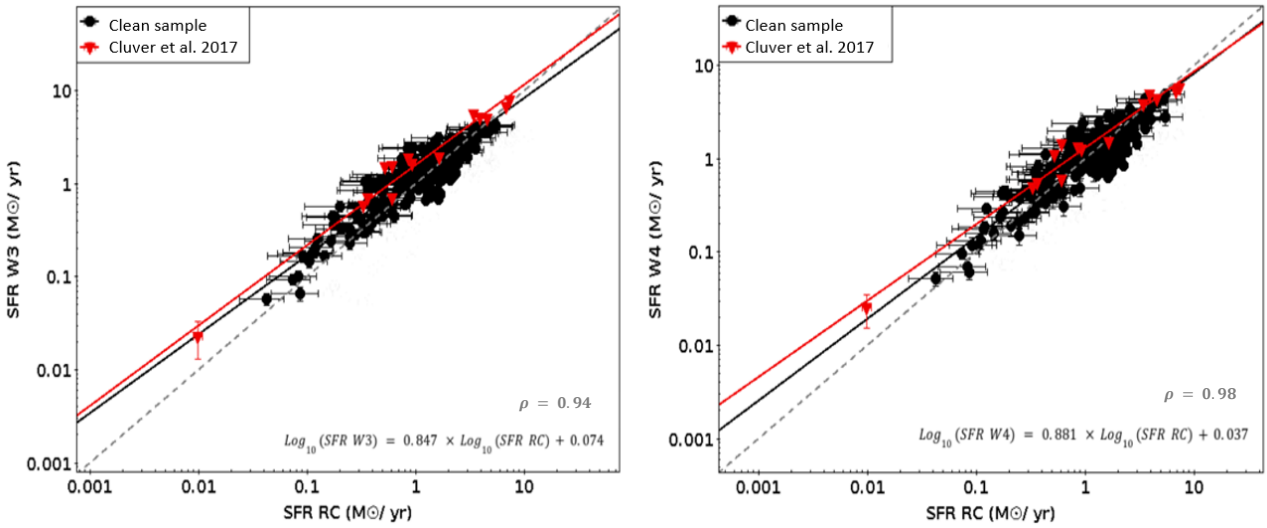

Figure 9: Plots of the SFR_{W3} vs SFR_{RC} and SFR_{W4} vs SFR_{RC} from left to right respectively. The red data points and fit are taken from Cluver et al. 2017. The black data points and fit, for which I give the expression, and the correlation factor belong to the clean galaxy sample. The dashed gray line is a one to one relation for reference.

Table 1: Best fits of the clean sample of this study and the reference sample of Cluver et al. 2017

	SFR_{W3} VS SFR_{RC}	SFR_{W4} VS SFR_{RC}
CLUVER ET AL 2017	$Log_{10}(SFR\ W3) = 0.842 \times Log_{10}(SFR\ RC) + 0.21$ ± 0.072 ± 0.04	$Log_{10}(SFR\ W4) = 0.845 \times Log_{10}(SFR\ RC) + 0.12$ ± 0.087 ± 0.05
CLEAN SAMPLE	$Log_{10}(SFR\ W3) = 0.847 \times Log_{10}(SFR\ RC) + 0.074$ ± 0.015 ± 0.08	$Log_{10}(SFR\ W4) = 0.881 \times Log_{10}(SFR\ RC) + 0.037$ ± 0.019 ± 0.06

I now analyze how the IR SFRs corrected using FUV values (SFR_{mircor}) correlate to SFR_{RC}. In particular, in the plot in Figure 10, I visualize both the clean and full samples to better understand the effect of this normalization. Clearly, the major impact of the correction is on the smaller SFR measurements, typical of lower mass galaxies, which increase significantly. Therefore, when considering that the IR tracers (at W3 and W4) might be underestimating SFRs due to the lower dust extinction in small sources, the trend deviates dramatically from the one to one line in the left end. The slope of the fit for the clean sample is 0.631 ± 0.010.

As expected, the FUV normalization works at the low mass regimes but it has a very little or no effect at the intermediate/higher ones. The main idea is that the dust amount and opacity of fainter objects are insufficient in absorbing the UV light of newborn stars and re-emitting that into the IR range.

Overall, data points look closely distributed along the linear fit, as suggested by the Pearson correlation coefficient of 0.94 and the estimated offset of 0.10.

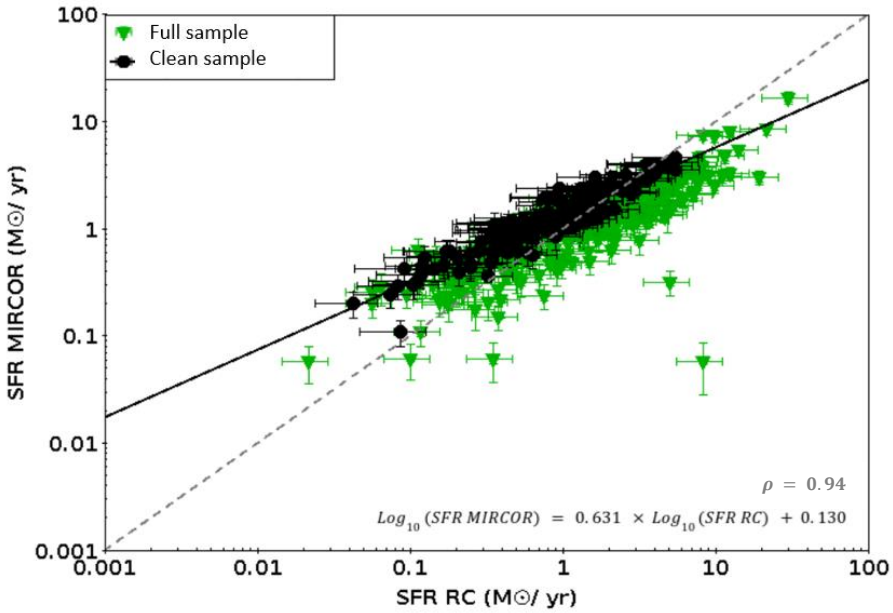

Figure 10: Plot of the SFR_{mircor} vs SFR_{RC}. The green data points represent the initial complete sample. The black data points and the fit, for which I give the expression, and the correlation factor refer to sources of the clean galaxy sample. The dashed black line is a one to one relation for reference.

4.4 IR vs FUV SFR

In Figure 11, I show the relations between IR SFRs (SFR_{W3}, SFR_{W4}) with the FUV derived ones (SFR_{FUV}), comparing the behavior of the clean and the full samples. In both plots, the distributions of data points appear very scattered. For the clean sample, this is also suggested by the estimated offsets to the best fits of 0.35 and 0.36 respectively. The linear correlations of data points are not strong as suggested by the Pearson correlation coefficients, of 0.51 and 0.49 respectively. The found linear fits deviate totally from the one to one line.
At small SFRs the W3 and W4 appear to measure more SF than the FUV, contrary to the expectations. In fact, smaller values should be better traced by the FUV for the reason explained in the previous paragraph. The possible reason for the very big discrepancy might be that FUV tracer is affected by dust or FUV data are not very accurate.

In Figure 12, I present the relation between SFR_{mircor} and SFR_{FUV} for the full and clean samples. The FUV normalization makes data points increase at lower values. In this case, the scatter is less than with the previous IR tracers (W3, W4) and, for the clean sample, this is also suggested by the smaller offset to the best fit, of 0.25. Also in this case, the linear correlation is not very strong as suggested by the Pearson coefficient (0.48).

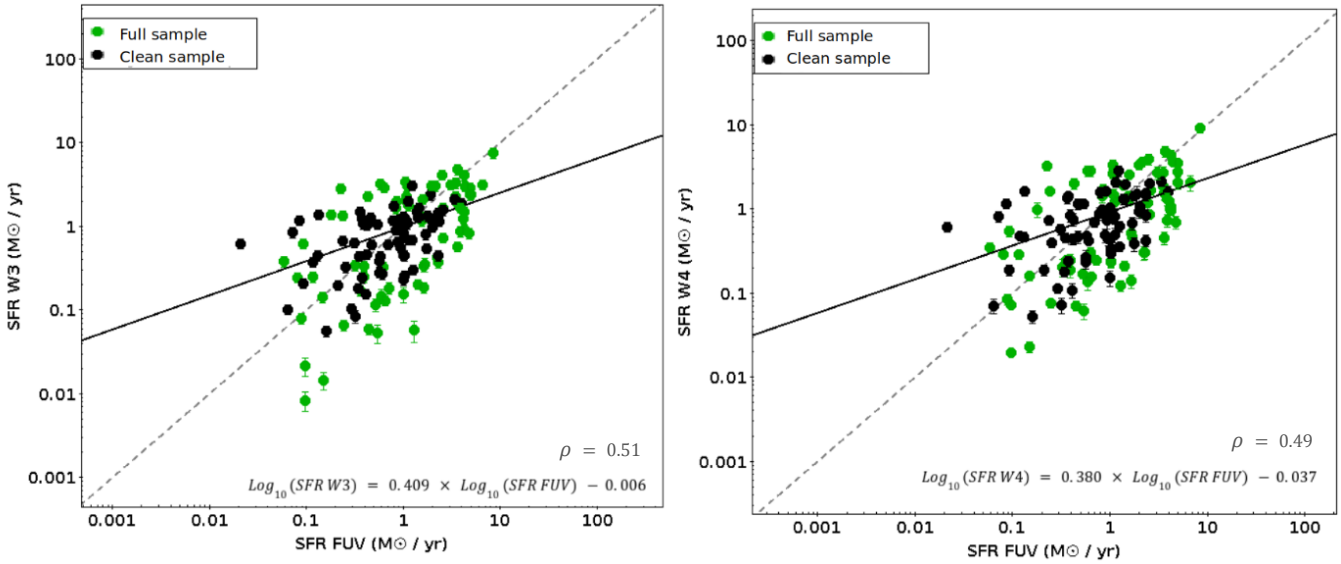

Figure 11: In the left panel is the plot of SFR_{W3} vs SFR_{FUV} while in the right panel of SFR_{W4} vs SFR_{FUV}. The green data points represent the initial complete sample. The black data points and the fit, for which I give the expression, and the correlation factor refer to sources of the clean galaxy sample. The dashed black line is a one to one relation for reference.

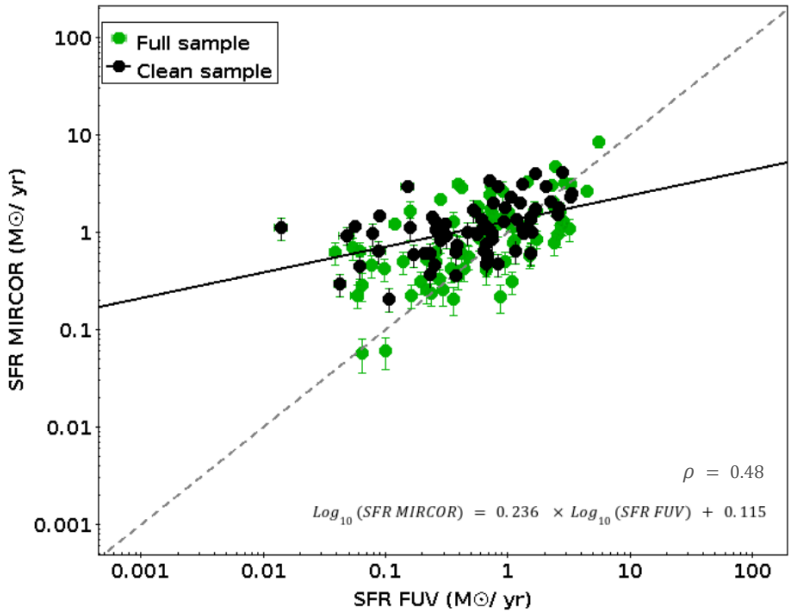

Figure 12: In this panel is the plot of SFR_{mircor} vs SFR_{FUV}, the green data points represent the complete sample. The black data points and the fit, for which I give the expression, and the correlation factor refer to sources of the clean galaxy sample. The dashed black line is a one to one relation for reference.

4.5 RC vs FUV SFR

In this last section of results, I present the relation between SFR_{FUV} and SFR_{RC} (Figure 13) for both the full and the clean samples.

Here, data points have less vertical scatter than in the case of correlations between IR SFRs at W3 and W4 vs SFR_{FUV} (Figure 11). This is suggested by the offset to the best fit of 0.33. Still the linear fit is far from the one to one line, with a slope of 0.473 ± 0.113. The overall trend shows that $SFR_{RC} > SFR_{FUV}$ in both samples, with a very few data points well related (on the one to one line). Also in this case, the discrepancy of the two tracers is clear; the RC based SFR might be more reliable than the FUV counterpart as the latter is affected by dust extinction while the radio band is not.

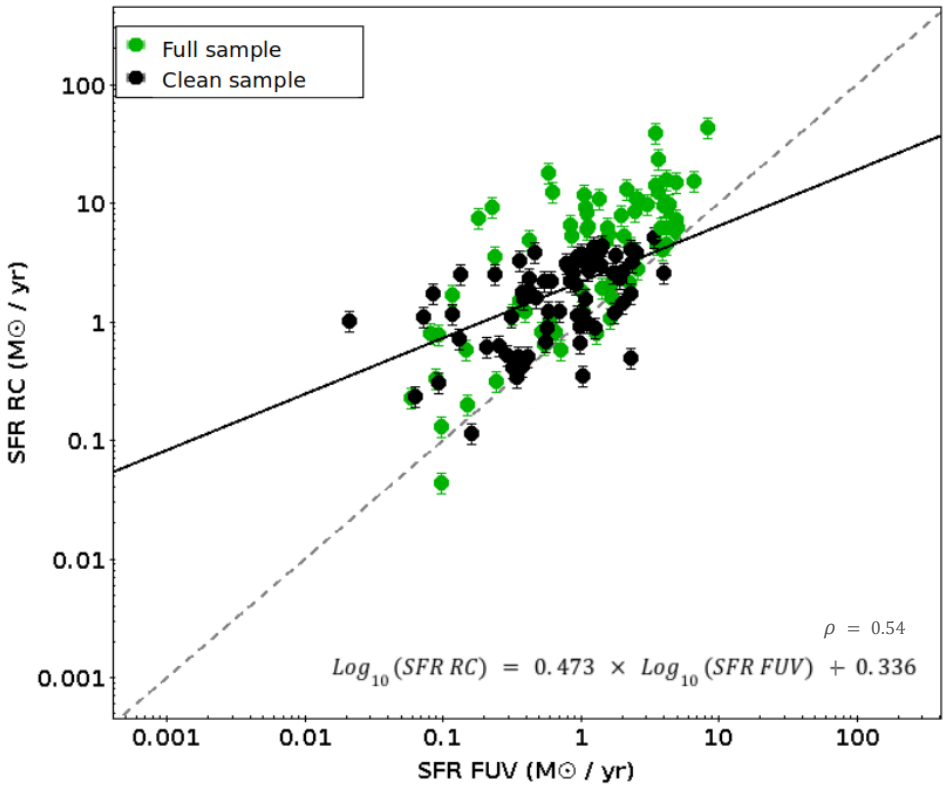

Figure 13: Plot of the SFR_{FUV} vs SFR_{RC}. The green data points represent the complete sample. The black data points and the fit, for which I give the expression, and the correlation factor refer to sources of the clean galaxy sample. The dashed black line is a one to one relation for reference.

CHAPTER 5: DISCUSSION

5.1 LACK OF DWARF GALAXIES IN SAMPLE

The improved WXSC W1 fluxes, good tracers of galaxy stellar masses, as well as the new calibrated mass relations provided in Jarrett et al. 2023, revealed the galaxy sample of this study to be less dwarf dominated than I expected and than I previously found using ALLWISE data. The possible reason for this might be the sample selection itself; requiring both a higher redshift and a radio continuum footprint in galaxies must have excluded the smaller ones, with a fainter radio continuum. In order to include as much dwarf galaxies as possible, this study could be performed starting from different initial conditions, i.e. without the lower distance cutoff or placing requirements for the RC, using improved Apertif data products or larger samples.

5.2 CONTAMINATED SOURCES

WISE contaminated sources can be easy to identify, as there are clearly objects that lie on top of the specific source of interest. Sometimes, also faint but very close objects might be considered as contaminating.

Radio contaminations appear with blended or spread RC contours that extend more than the galaxy shape. Occasionally, the radio seems displaced from the selected objects suggesting it is not really tracing SF activity in that source.

RC and WISE contaminated objects, as plotted in Figure 8 (SFR_{W3} vs SFR_{RC} & SFR_{W4} vs SFR_{RC}), are spread in the whole distributions of data points, without a clear separation. As anticipated in the previous section, the overlap might be due to the radio contamination adding extra radio flux thus increasing RC SFRs as well as the mask of contaminating sources in WISE images, which results in artificially lower measured fluxes hence, lower IR SFRs.

5.3 FIR-RADIO SFR CORRELATIONS

Preliminarily, I explored the relation of IR SFRs with the stellar masses of galaxies. In particular in the plot Log $sSFR_{mir}$ vs Log stellar mass, in Figure 7, there is a flat distribution of data points. Instead, in the plot Log $sSFR_{mircor}$ vs Log stellar mass, a small trend appears with lower mass galaxies forming relatively more stars per unit mass than the more massive ones. This suggests that the FUV normalization has a greater impact on low mass galaxies, making their SFRs significantly increase.

As known from the literature (Jarrett et al. 2017), the MIR and FIR WISE W3 and W4 bands are optimal tracers of recent star formation as, unlike W1 and W2, they are not polluted by old stars: W3 captures atomic and molecular lines and continuum emission while W4 is sensitive to the continuum of small dust grains. As shown in section 4.3, these IR monochromatic tracers work well for the clean sample and agree reasonably with the SFR_{RC}. Additionally, the found correlations are almost consistent with those of Cluver et al. 2017, as shown in the comparing table of the same section. In this work, there is a tight correlation between SFR_{W4} and SFR_{RC}. This last good agreement leads to the conclusion that SF is better traced in W4 than in W3. And this suggests that dust extinction has a great impact on the star-forming environment

of the selected sources; therefore, most of the UV light emitted by freshly formed stars is reprocessed by dust and emitted in a frequency range that corresponds to the WISE W4.

However, in the trend SFR_{mircor} vs SFR_{RC}, in Figure 10, the good correlation breaks at smaller SFR values. This is a consequence of the FUV normalization that specifically targets low SFRs, typically found in galaxies with a little dust. Data points at small values are thus found prominently above the one to one line whereas, the higher ones remain almost untouched, as they are not impacted by the FUV normalization. This suggests that, on the one hand, both SFR_{W3} and SFR_{W4} might be underestimating the smaller SFRs. In fact, at such regimes, IR tracers are questionable on the basis of a lack of copious dust, optically thin and not efficient is absorbing the starlight. In addition, the small size and dust opacity of low mass galaxies could result in a suppressed radio emission (Bell E.F. 2003); the possible reason might be that cosmic ray electrons accelerated by supernovae escape the galaxy before undergoing energy loss (Heesen et al. 2022). On the other hand, the consistency of the FUV normalization should be better tested in a sample dominated by low mass sources.

5.4 COMPARISON WITH FUV SFRS

Given the discrepancy between WISE & RC SFRs the idea was to use FUV as another tracer to see if it could determine which was a better tracer - was SFR_{RC} under-predicting or SFR_{mircor} over-predicting at lower SFR values?

In the plot SFR_{W3} and SFR_{W4} vs SFR_{FUV}, in Figure 11, I would have expected a majority of small SFR values in the clean sample to have a higher SFR measured by FUV. They, instead, are very scattered and they have higher IR values. This might be due to limitations related to dust extinction effects as well as to the UV photometric measurements. In fact, GALEX source catalog is point-source optimized, like ALLWISE. Therefore, UV fluxes would increase with a proper extended source photometry and this would possibly result in a more clear trend, especially at low SFRs at which FUV is expected to be higher, allowing more accurate analyses.

In the comparison of SFR_{mircor} vs SFR_{FUV}, in Figure 12, the *mircor* values are intrinsically higher in the lower range. But this is just how this FUV normalization is built; its consistency has to be well assessed in a more expanded sample including a fair number of lower mass galaxies.

In the comparison SFR_{FUV} vs SFR_{RC}, in Figure 13, the FUV appears clearly underestimated.

The main consideration is that FUV data was not useful in helping determine which SF calibration to trust at the lower SFRs, where we saw the large discrepancies. This is due to limitations of GALEX photometry as well as the availability of an insufficient amount of FUV information.

CHAPTER 6: CONCLUSIONS

Thanks to improved WXSC data (T. Jarrett, priv. comm.) and the sensitive Apertif data products, I could do a study of the FIR-Radio SFR correlations for the HI – radio selected sources.

Initially, the aim was to study the reliability of radio SF tracers in dwarf galaxies. When I first estimated the stellar masses using ALLWISE W1 fluxes, the sample resulted to contain a fair number (37/250) of low mass galaxies with $M < 10^9\ M_\odot$. However, using the improved IR photometry (WXSC) only 9 were confirmed in that mass range. Therefore, in absence of a good number of dwarfs, the analysis turned out to be a study of the FIR-Radio correlation for intermediate, high mass galaxies, in the range $10^9\ M_\odot < M < 10^{12}\ M_\odot$.

With the visual inspection, I identified a clean sample of objects for which I believe there is a good agreement between IR and radio traced star forming activity; I put my focus on these galaxies to compare SFRs at different bands.

Whereas SFR_{W3} and SFR_{W4} seem to reasonably correlate to the SFR_{RC}, there is a big discrepancy at smaller values when using SFR_{mircor} vs SFR_{RC}. The question now is: which is more reliable? The IR SFR tracers at W3 and W4 may underestimate SF at small regimes because of the lower dust content and opacity; these might also cause a suppressed radio emission. Since the FUV is expected to be consistent at smaller SF values, the point becomes: will the FUV tracer clarify whether to trust more the corrected MIR SFRs over the individual W3, W4 and also RC derived ones?

However, possible limitations of the FUV photometry as well as the unavailability of a consistent amount of FUV data did not allow answering this question. As it remains an open question, further investigations are needed and they would explicitly benefit from a sample enriched in low mass sources.

Overall, to focus the study on low mass galaxies the sample selection should not include the redshift cut-off; moreover, the use of improved Apertif data products could help find a larger number of radio faint objects.

REFERENCES

Adams, E. A. K., Adebahr, B., de Blok, W. J. G., Dénes, H., Hess, K. M., van der Hulst, J. M., Kutkin, A., Lucero, D. M., Morganti, R., Moss, V. A., Oosterloo, T. A., Orrú, E., Schulz, R., van Amesfoort, A. S., Berger, A., Boersma, O. M., Bouwhuis, M., van den Brink, R., van Cappellen, W. A., … Ziemke, J. (2022). First release of Apertif imaging survey data. *Astronomy & Astrophysics*, *667*, A38. https://doi.org/10.1051/0004-6361/202244007

Bell, E. F. (2003). Estimating Star Formation Rates from Infrared and Radio Luminosities: The Origin of the Radio-Infrared Correlation. *The Astrophysical Journal*, *586*(2), 794–813. https://doi.org/10.1086/367829

Bianchi, L., Shiao, B., & Thilker, D. (2017). Revised Catalog of *GALEX* Ultraviolet Sources. I. The All-Sky Survey: GUVcat_AIS. *The Astrophysical Journal Supplement Series*, *230*(2), 24. https://doi.org/10.3847/1538-4365/aa7053

Buat, V., Boselli, A., Gavazzi, G., & Bonfanti, C. (2002). Star formation and dust extinction in nearby star-forming and starburst galaxies. *Astronomy & Astrophysics*, *383*(3), 801–812. https://doi.org/10.1051/0004-6361:20011832

Burgarella, D., Nanni, A., Hirashita, H., Theulé, P., Inoue, A. K., & Takeuchi, T. T. (2020). Observational and theoretical constraints on the formation and early evolution of the first dust grains in galaxies at 5 < *z* < 10. *Astronomy & Astrophysics*, *637*, A32. https://doi.org/10.1051/0004-6361/201937143

Calzetti, D. (2001). The Dust Opacity of Star-forming Galaxies. *Publications of the Astronomical Society of the Pacific*, *113*(790), 1449–1485. https://doi.org/10.1086/324269

Calzetti, D., Kennicutt, R. C., Engelbracht, C. W., Leitherer, C., Draine, B. T., Kewley, L., Moustakas, J., Sosey, M., Dale, D. A., Gordon, K. D., Helou, G. X., Hollenbach, D. J., Armus, L., Bendo, G., Bot, C., Buckalew, B., Jarrett, T., Li, A., Meyer, M., … Walter, F. (2007). The Calibration of Mid-Infrared Star Formation Rate Indicators. *The Astrophysical Journal*, *666*(2), 870–895. https://doi.org/10.1086/520082

Calzetti, D. (2012). *Star Formation Rate Indicators*.

Carigi, L., & Peimbert, M. (2011). *Solar origins: Place and Chemical Composition*.

Cattaneo, A., Mamon, G. A., Warnick, K., & Knebe, A. (2011). How do galaxies acquire their mass? *Astronomy & Astrophysics*, *533*, A5. https://doi.org/10.1051/0004-6361/201015780

Chi, X., Szabelski, J., Vahia, M. N., Wdowczyk, J., & Wolfendale, A. W. (1992). Cosmic rays of the highest energies: I. Evidence for a galactic component. *Journal of Physics G: Nuclear and Particle Physics*, *18*(3), 539–552. https://doi.org/10.1088/0954-3899/18/3/008

Cluver, M. E., Jarrett, T. H., Dale, D. A., Smith, J.-D. T., August, T., & Brown, M. J. I. (2017). Calibrating Star Formation in *WISE* Using Total Infrared Luminosity. *The Astrophysical Journal*, *850*(1), 68. https://doi.org/10.3847/1538-4357/aa92c7

Cole, S., Lacey, C., Baugh, C., & Frenk, C. (2000). *Hierarchical Galaxy Formation*. https://doi.org/10.1046/j.1365-8711.2000.03879.x

Condon, J. J. (1992). Radio Emission from Normal Galaxies. *Annual Review of Astronomy and Astrophysics*, *30*(1), 575–611. https://doi.org/10.1146/annurev.aa.30.090192.003043

Conselice, C. J., Wilkinson, A., Duncan, K., & Mortlock, A. (2016). *The Evolution of Galaxy Number Density at z < 8 and its Implications*. https://doi.org/10.3847/0004-637X/830/2/83

Cross, N. J. G., Driver, S. P., Liske, J., Lemon, D. J., Peacock, J. A., Cole, S., Norberg, P., & Sutherland, W. J. (2004). The Millennium Galaxy Catalogue: the photometric accuracy, completeness and contamination of the 2dFGRS and SDSS-EDR/DR1 data sets. *Monthly Notices of the Royal Astronomical Society*, *349*(2), 576–594. https://doi.org/10.1111/j.1365-2966.2004.07527.x

Ferguson, H. C., & Binggeli, B. (1994). Dwarf elliptical galaxies. *The Astronomy and Astrophysics Review*, *6*(1–2), 67–122. https://doi.org/10.1007/BF01208252

Han, J. L., Beck, R., & Berkhuijsen, E. M. (1998). *New clues to the magnetic field structure of M31*.

Heesen, V., Brinks, E., Leroy, A. K., Heald, G., Braun, R., Bigiel, F., & Beck, R. (2014). THE RADIO CONTINUUM-STAR FORMATION RATE RELATION IN WSRT SINGS GALAXIES. *The Astronomical Journal*, *147*(5), 103. https://doi.org/10.1088/00046256/147/5/103

Heesen, V., Staffehl, M., Basu, A., Beck, R., Stein, M., Tabatabaei, F. S., Hardcastle, M. J., Chyży, K. T., Shimwell, T. W., Adebahr, B., Beswick, R., Bomans, D. J., Botteon, A., Brinks, E., Brüggen, M., Dettmar, R.-J., Drabent, A., de Gasperin, F., Gürkan, G., … Tasse, C. (2022). Nearby galaxies in the LOFAR Two-metre Sky Survey. *Astronomy & Astrophysics*, *664*, A83. https://doi.org/10.1051/0004-6361/202142878

Helou, G., Soifer, B. T., & Rowan-Robinson, M. (1985). Thermal infrared and nonthermal radio - Remarkable correlation in disks of galaxies. *The Astrophysical Journal*, *298*, L7. https://doi.org/10.1086/184556

Hernquist, L., & Mihos, C. (1995). *Excitation of Activity in Galaxies by Minor Mergers*. https://doi.org/10.1086/175940

Hoffman, G. L., Salpeter, E. E., Farhat, B., Roos, T., Williams, H., & Helou, G. (1996). *Arecibo HI Mapping of a Large Sample of Dwarf Irregular Galaxies*. https://doi.org/10.1086/192314

Hubble, E. P. (1926). Extragalactic nebulae. *The Astrophysical Journal*, *64*, 321. https://doi.org/10.1086/143018

Jarrett, T. H., Cluver, M. E., Taylor, E. N., Bellstedt, S., Robotham, A. S. G., & Yao, H. F. M. (2023). A New Wide-field Infrared Survey Explorer Calibration of Stellar Mass. *The Astrophysical Journal*, *946*(2), 95. https://doi.org/10.3847/1538-4357/acb68f

Jarrett, T. H., Masci, F., Tsai, C. W., Petty, S., Cluver, M. E., Assef, R. J., Benford, D., Blain, A., Bridge, C., Donoso, E., Eisenhardt, P., Koribalski, B., Lake, S., Neill, J. D., Seibert, M., Sheth, K., Stanford, S., & Wright, E. (2013). EXTENDING THE NEARBY GALAXY HERITAGE WITH *WISE* : FIRST RESULTS FROM THE *WISE* ENHANCED RESOLUTION GALAXY ATLAS. *The Astronomical Journal*, *145*(1), 6. https://doi.org/10.1088/0004-6256/145/1/6

Jarrett, T. H., Cluver, M. E., Brown, M. J. I., Dale, D. A., Tsai, C. W., & Masci, F. (2019). *The WISE Extended Source Catalogue (WXSC) I: The 100 Largest Galaxies*. https://doi.org/10.3847/1538-4365/ab521a

Kennicutt, , Robert C. (1998). *Star Formation in Galaxies Along the Hubble Sequence*. https://doi.org/10.1146/annurev.astro.36.1.189

Kennicutt, R. C., Hao, C.-N., Calzetti, D., Moustakas, J., Dale, D. A., Bendo, G., Engelbracht, C. W., Johnson, B. D., & Lee, J. C. (2009). DUST-CORRECTED STAR FORMATION RATES OF GALAXIES. I. COMBINATIONS OF Hα AND INFRARED TRACERS. *The Astrophysical Journal*, *703*(2), 1672–1695. https://doi.org/10.1088/0004-637X/703/2/1672

Kewley, L. J., Geller, M. J., Jansen, R. A., & Dopita, M. A. (2002). The Hα and Infrared Star Formation Rates for the Nearby Field Galaxy Survey. *The Astronomical Journal*, *124*(6), 3135–3143. https://doi.org/10.1086/344487

Kroupa, P., Tout, C. A., & Gilmore, G. (1993). The distribution of low-mass stars in the Galactic disc. *Monthly Notices of the Royal Astronomical Society*, *262*(3), 545–587. https://doi.org/10.1093/mnras/262.3.545

Kutkin, A. M., Oosterloo, T. A., Morganti, R., Adams, E. A. K., Mancini, M., Adebahr, B., de Blok, W. J. G., Dénes, H., Hess, K. M., van der Hulst, J. M., Lucero, D. M., Moss, V. A., Berger, A., van den Brink, R., van Cappellen, W. A., Connor, L., Damstra, S., Loose, G. M., van Leeuwen, J., … Ziemke, J. (2022). Continuum source catalog for the first APERTIF data release. *Astronomy & Astrophysics*, *667*, A39. https://doi.org/10.1051/0004-6361/202244008

Lee, J. C., Gil de Paz, A., Tremonti, C., Kennicutt, R. C., Salim, S., Bothwell, M., Calzetti, D., Dalcanton, J., Dale, D., Engelbracht, C., José G. Funes, S. J., Johnson, B., Sakai, S., Skillman, E., van Zee, L., Walter, F., & Weisz, D. (2009). COMPARISON OF Hα AND UV STAR FORMATION RATES IN THE LOCAL VOLUME: SYSTEMATIC DISCREPANCIES FOR DWARF GALAXIES. *The Astrophysical Journal*, *706*(1), 599–613. https://doi.org/10.1088/0004-637X/706/1/599

Lee, J. C., Veilleux, S., McDonald, M., & Hilbert, B. (2016). A DEEPER LOOK AT FAINT H α EMISSION IN NEARBY DWARF GALAXIES. *The Astrophysical Journal*, *817*(2), 177. https://doi.org/10.3847/0004-637X/817/2/177

Leitherer, C., Schaerer, D., Goldader, J. D., Delgado, R. M. G., Robert, C., Kune, D. F., de Mello, D. F., Devost, D., & Heckman, T. M. (1999). *Starburst99: Synthesis Models for Galaxies with Active Star Formation*. https://doi.org/10.1086/313233

Malcolm S. Longair. (2007). *Galaxy Formation* (2007 Springer Science & Business Media, Ed.; 2nd, illustrata ed.).

Ogle, P. M., Jarrett, T., Lanz, L., Cluver, M., Alatalo, K., Appleton, P. N., & Mazzarella, J. M. (2019). A Break in Spiral Galaxy Scaling Relations at the Upper Limit of Galaxy Mass. *The Astrophysical Journal*, *884*(1), L11. https://doi.org/10.3847/2041-8213/ab459e

Price, R., & Duric, N. (1992). New results on the radio-far-infrared relation for galaxies. *The Astrophysical Journal*, *401*, 81. https://doi.org/10.1086/172040

Radcliffe, J. F., Barthel, P. D., Garrett, M. A., Beswick, R. J., Thomson, A. P., & Muxlow, T. W. B. (2021). The radio emission from active galactic nuclei. *Astronomy & Astrophysics*, *649*, L9. https://doi.org/10.1051/0004-6361/202140791

Reddy, N. A., Kriek, M., Shapley, A. E., Freeman, W. R., Siana, B., Coil, A. L., Mobasher, B., Price, S. H., Sanders, R. L., & Shivaei, I. (2015). THE MOSDEF SURVEY: MEASUREMENTS OF BALMER DECREMENTS AND THE DUST ATTENUATION CURVE AT REDSHIFTS $z \sim 1.4$–2.6. *The Astrophysical Journal*, *806*(2), 259. https://doi.org/10.1088/0004-637X/806/2/259

Salim, S., Boquien, M., & Lee, J. C. (2018). Dust Attenuation Curves in the Local Universe: Demographics and New Laws for Star-forming Galaxies and High-redshift Analogs. *The Astrophysical Journal*, *859*(1), 11. https://doi.org/10.3847/1538-4357/aabf3c

Salpeter, E. E. (1955). The Luminosity Function and Stellar Evolution. *The Astrophysical Journal*, *121*, 161. https://doi.org/10.1086/145971

Schruba, A., Leroy, A. K., Walter, F., Bigiel, F., Brinks, E., de Blok, W. J. G., Dumas, G., Kramer, C., Rosolowsky, E., Sandstrom, K., Schuster, K., Usero, A., Weiss, A., & Wiesemeyer, H. (2011). A MOLECULAR STAR FORMATION LAW IN THE ATOMIC-GAS-DOMINATED REGIME IN NEARBY GALAXIES. *The Astronomical Journal*, *142*(2), 37. https://doi.org/10.1088/0004-6256/142/2/37

Simon, J. D. (2019). *The Faintest Dwarf Galaxies*. https://doi.org/10.1146/annurev-astro-091918-104453

Tolstoy, E., Hill, V., & Tosi, M. (2009). Star-Formation Histories, Abundances, and Kinematics of Dwarf Galaxies in the Local Group. *Annual Review of Astronomy and Astrophysics*, *47*(1), 371–425. https://doi.org/10.1146/annurev-astro-082708-101650

van Cappellen, W. A., Oosterloo, T. A., Verheijen, M. A. W., Adams, E. A. K., Adebahr, B., Braun, R., Hess, K. M., Holties, H., van der Hulst, J. M., Hut, B., Kooistra, E., van Leeuwen, J., Loose, G. M., Morganti, R., Moss, V. A., Orrú, E., Ruiter, M., Schoenmakers, A. P., Vermaas, N. J., … Ziemke, J. (2021). *Apertif, Phased Array Feeds for the Westerbork Synthesis Radio Telescope*. https://doi.org/10.1051/0004-6361/202141739

Vollmer, B., Soida, M., & Dallant, J. (2022). Deciphering the radio–star formation correlation on kpc scales. *Astronomy & Astrophysics*, *667*, A30. https://doi.org/10.1051/0004-6361/202142877

Wang, J., Heckman, T. M., & Lehnert, M. D. (1998). Toward a Unified Model for the “Diffuse Ionized Medium” in Normal and Starburst Galaxies. *The Astrophysical Journal*, *509*(1), 93–102. https://doi.org/10.1086/306489
Yun, M. S., Reddy, N. A., & Condon, J. J. (2001). Radio Properties of Infrared-Selected Galaxies in the *IRAS* 2 Jy Sample. *The Astrophysical Journal*, *554*(2), 803–822. https://doi.org/10.1086/323145

APPENDIX – VISUAL INSPECTION

Good data: Radio and IR emission from the source

J131549+564830

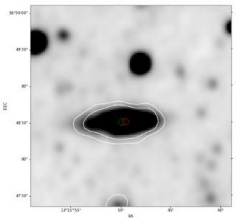

J131612+305700

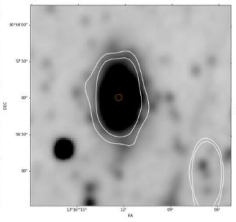

J015515+305006

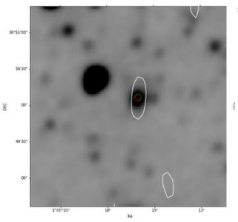

J015706+324721

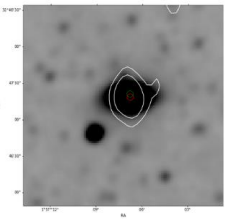

J101942+572524

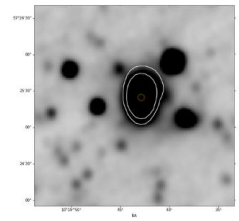

J102006+560612

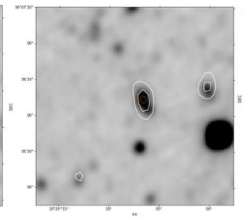

J102656+572423

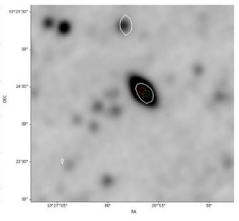

J101254+585153

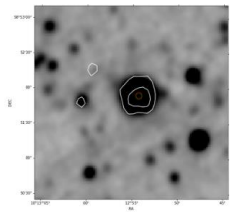

J020011.20+373613.1

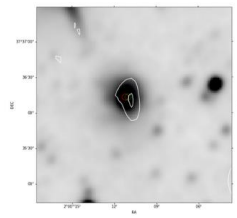

J105047+501008

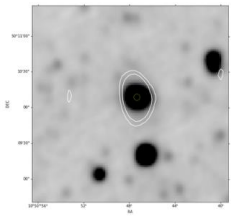

J110805+572148

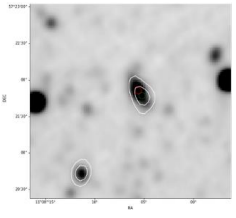

J110843+584614

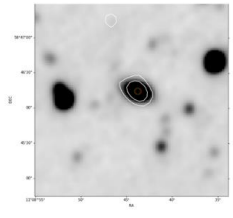

J014435+374146

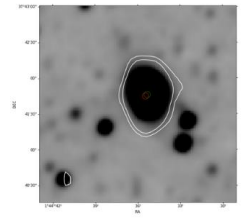

J015143+302306

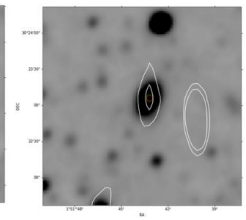

J130604+553921

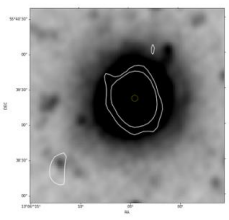

J130855+290227

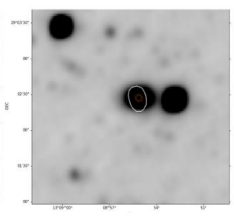

J111857+610421

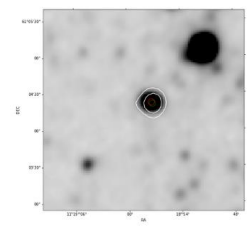

J130343+611903

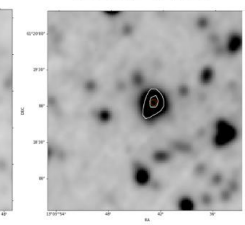

J131944+320558

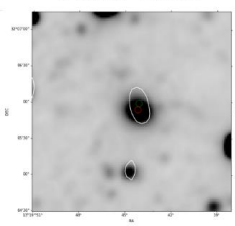

J132119+313309

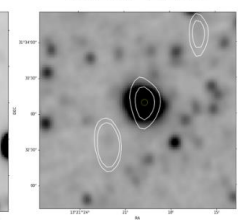

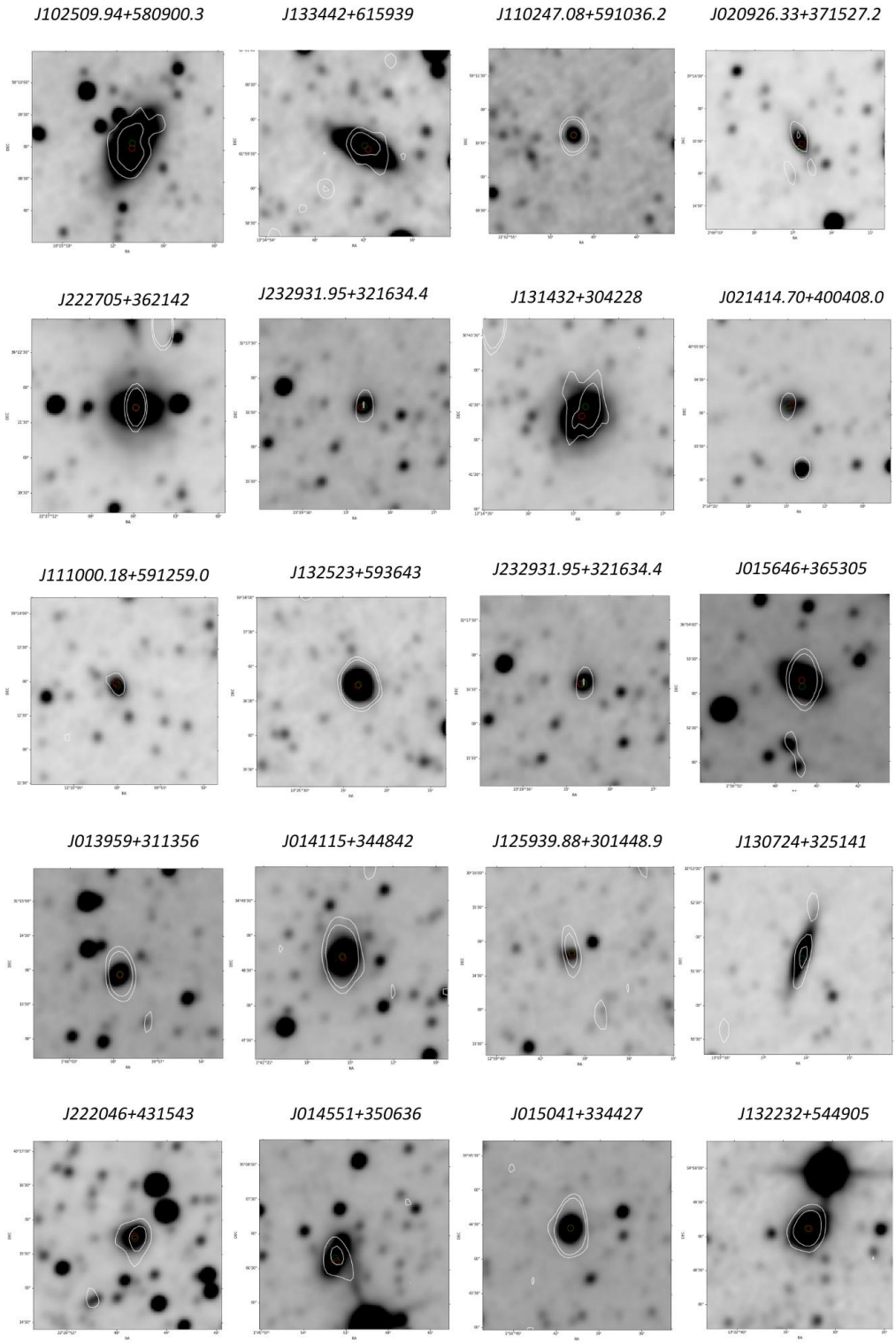
J102509.94+580900.3
J133442+615939
J110247.08+591036.2
J020926.33+371527.2
J222705+362142
J232931.95+321634.4
J131432+304228
J021414.70+400408.0
J111000.18+591259.0
J132523+593643
J232931.95+321634.4
J015646+365305
J013959+311356
J014115+344842
J125939.88+301448.9
J130724+325141
J222046+431543
J014551+350636
J015041+334427
J132232+544905

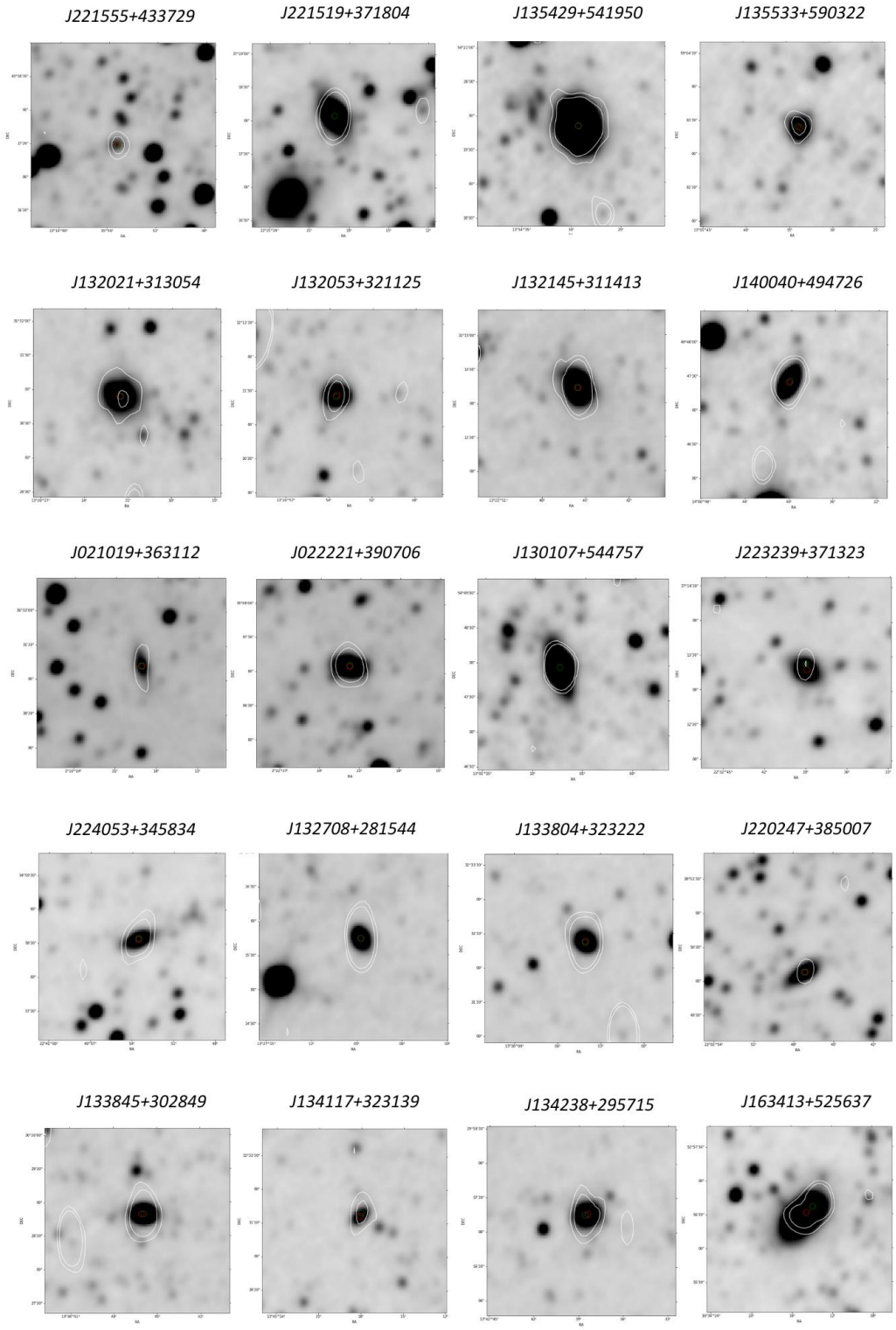
J221555+433729
J221519+371804
J135429+541950
J135533+590322
J132021+313054
J132053+321125
J132145+311413
J140040+494726
J021019+363112
J022221+390706
J130107+544757
J223239+371323
J224053+345834
J132708+281544
J133804+323222
J220247+385007
J133845+302849
J134117+323139
J134238+295715
J163413+525637

J223459+371159

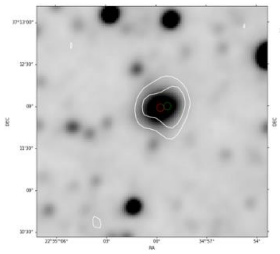

J140952+342205

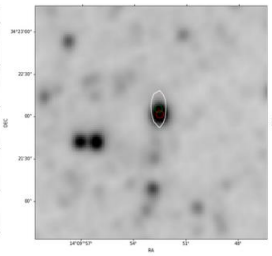

J141459+303634

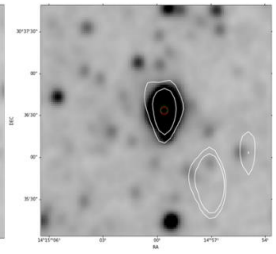

J221715+333012

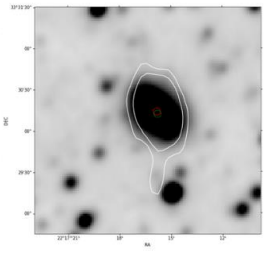

J220653+455846

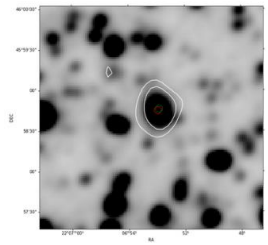

J221014+363919

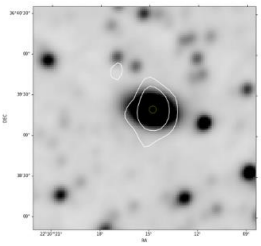

J221650+413006

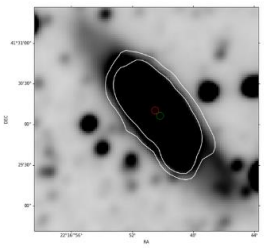

J222252+420251

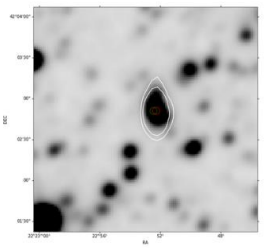

J221027+405913

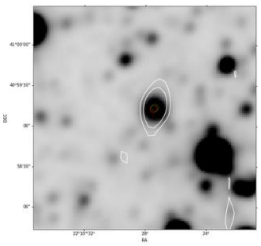

J221156+445438

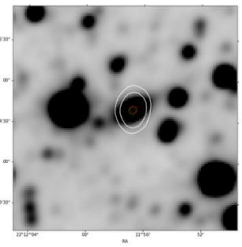

J221601+405208

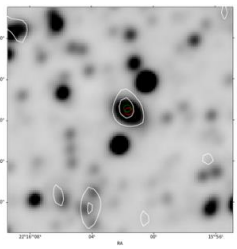

J222402+332611

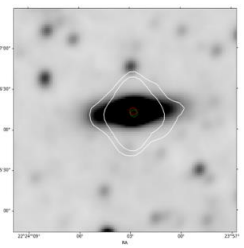

J222016+434914

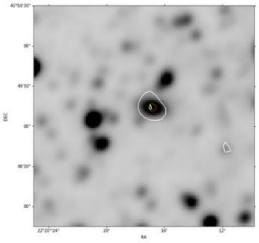

J222307+403246

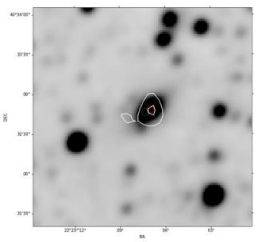

J221814+332441

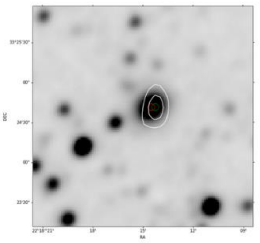

J223050+363347

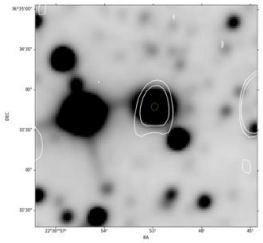

J221735+455829

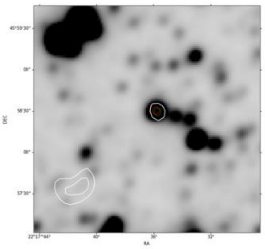

J222916+374507

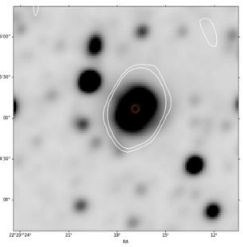

J222928+364700

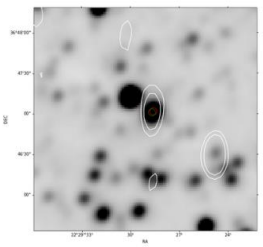

J222629+353143

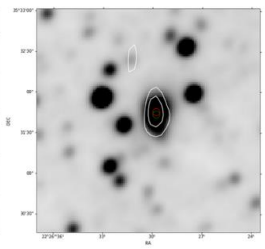

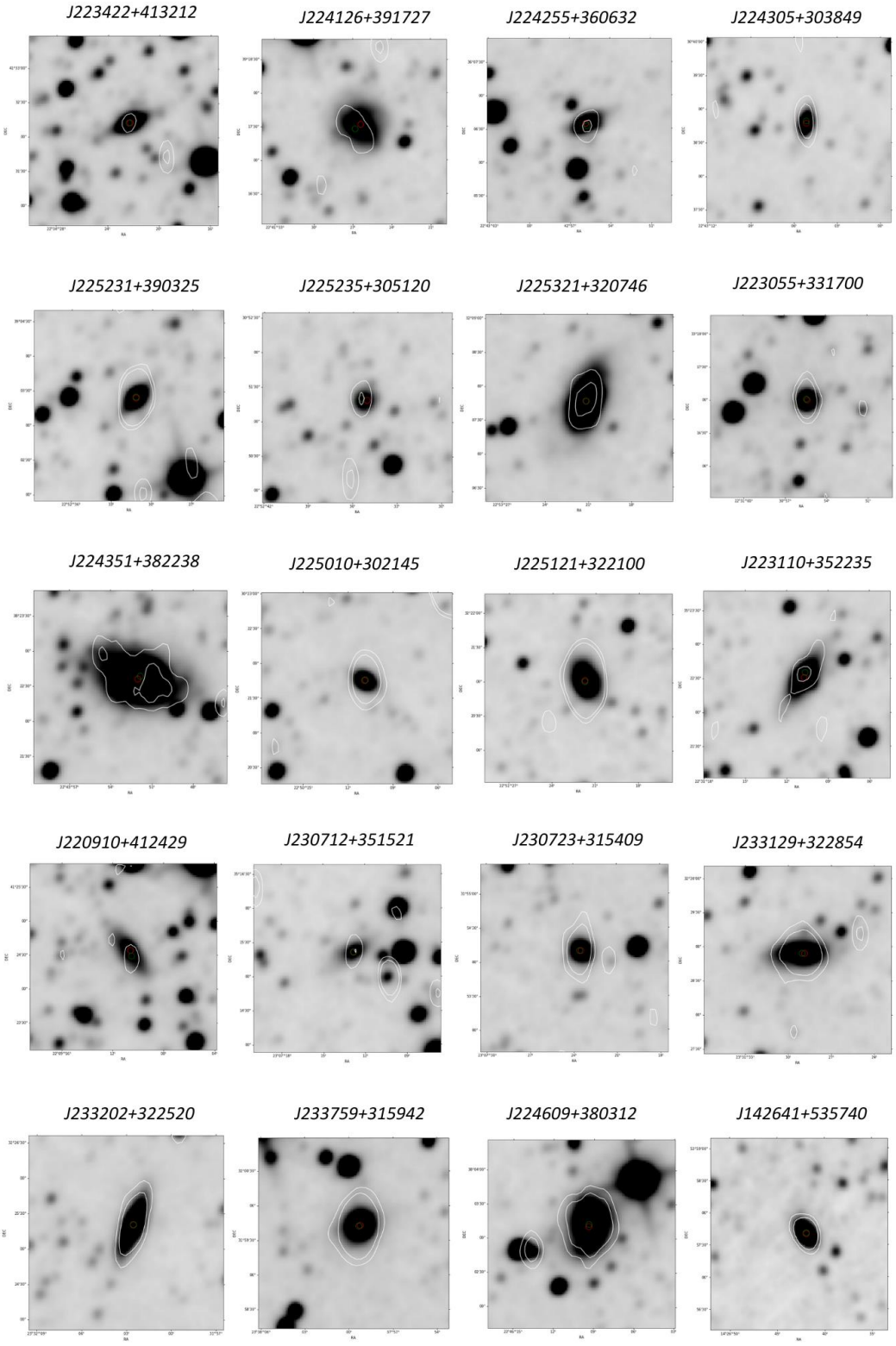
J223422+413212
J224126+391727
J224255+360632
J224305+303849
J225231+390325
J225235+305120
J225321+320746
J223055+331700
J224351+382238
J225010+302145
J225121+322100
J223110+352235
J220910+412429
J230712+351521
J230723+315409
J233129+322854
J233202+322520
J233759+315942
J224609+380312
J142641+535740

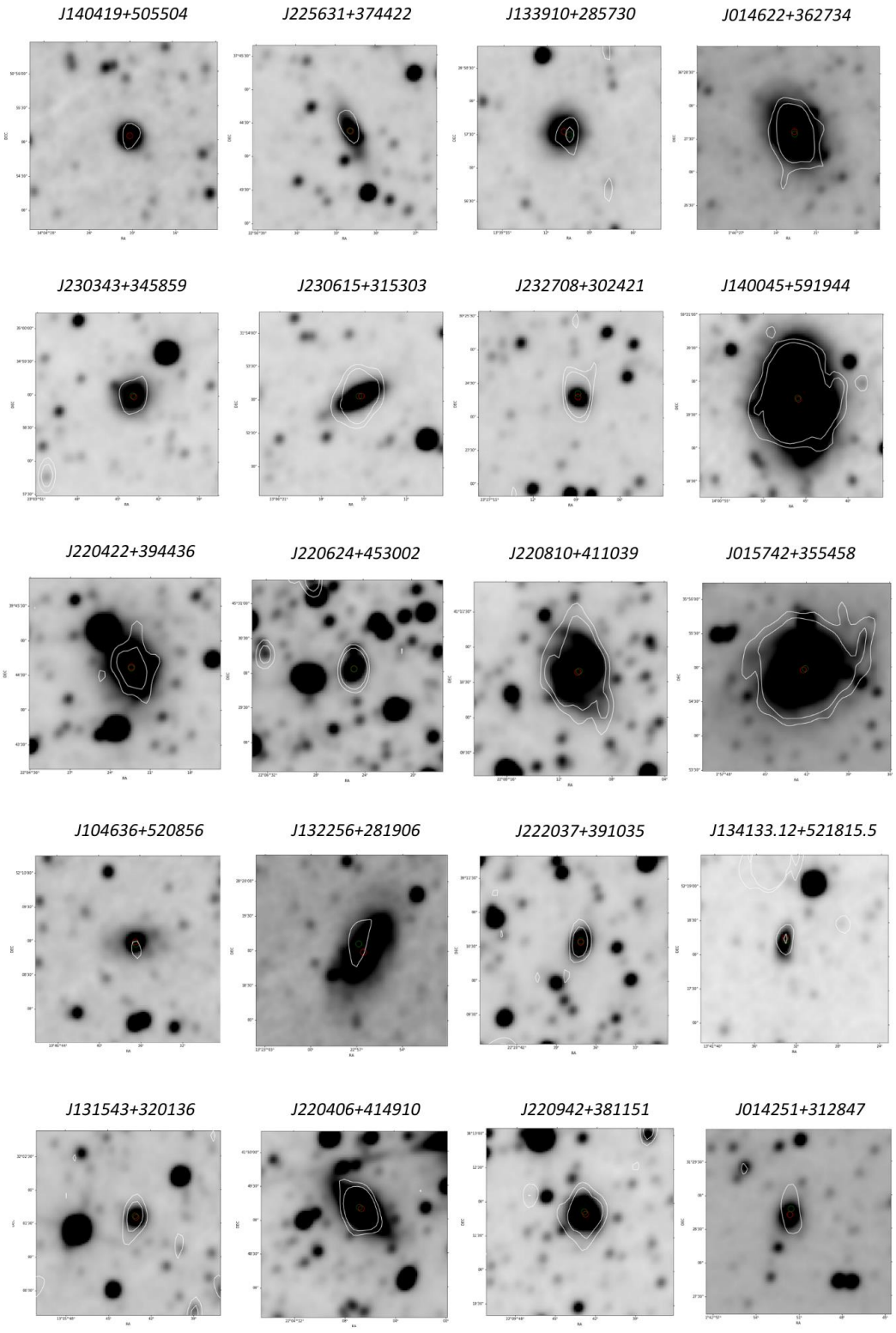
J140419+505504
J225631+374422
J133910+285730
J014622+362734
J230343+345859
J230615+315303
J232708+302421
J140045+591944
J220422+394436
J220624+453002
J220810+411039
J015742+355458
J104636+520856
J132256+281906
J222037+391035
J134133.12+521815.5
J131543+320136
J220406+414910
J220942+381151
J014251+312847

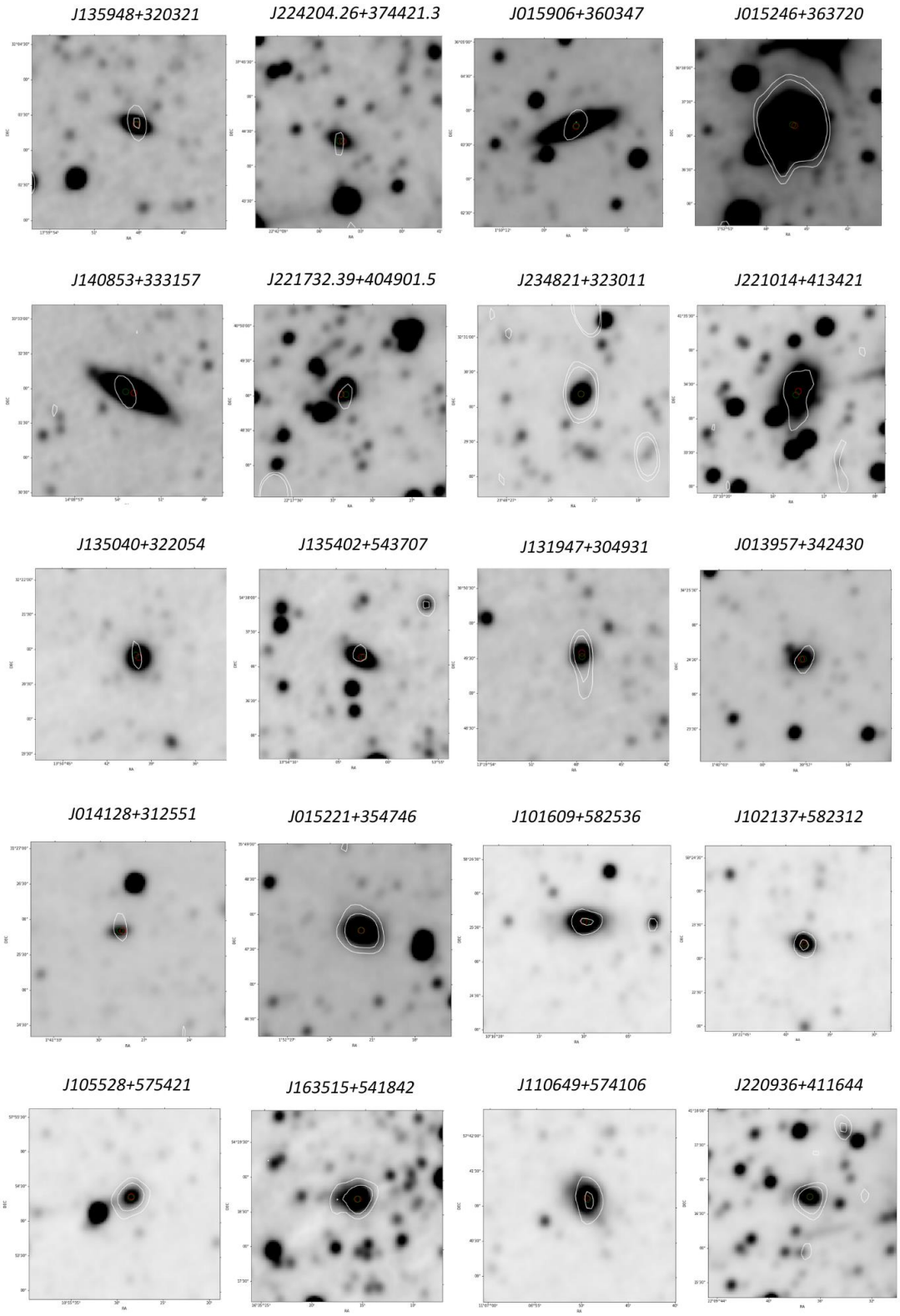
J135948+320321
J224204.26+374421.3
J015906+360347
J015246+363720
J140853+333157
J221732.39+404901.5
J234821+323011
J221014+413421
J135040+322054
J135402+543707
J131947+304931
J013957+342430
J014128+312551
J015221+354746
J101609+582536
J102137+582312
J105528+575421
J163515+541842
J110649+574106
J220936+411644

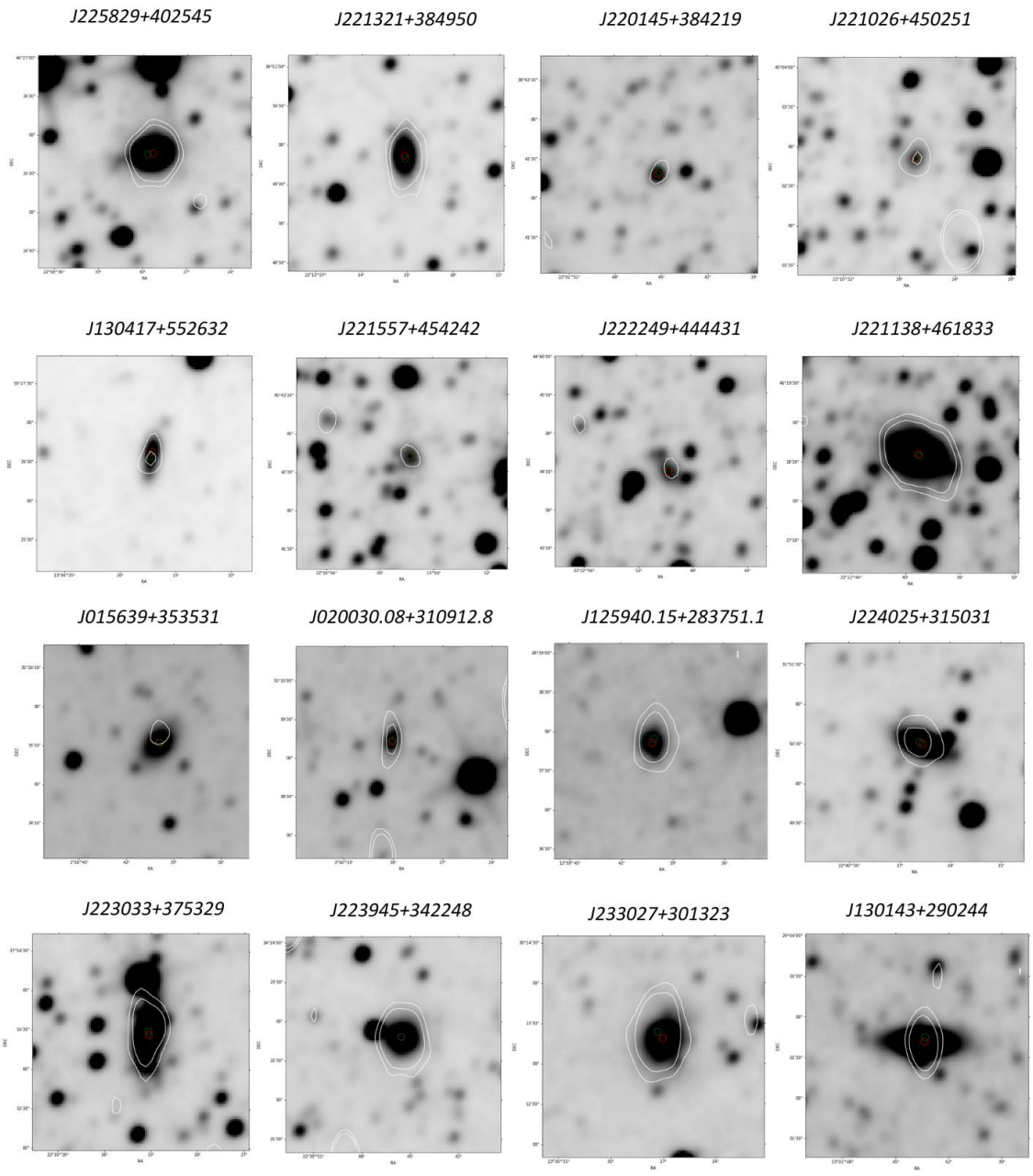
J225829+402545
J221321+384950
J220145+384219
J221026+450251
J130417+552632
J221557+454242
J222249+444431
J221138+461833
J015639+353531
J020030.08+310912.8
J125940.15+283751.1
J224025+315031
J223033+375329
J223945+342248
J233027+301323
J130143+290244

RADIO CONTAMINATION

J222249.71+444429.0

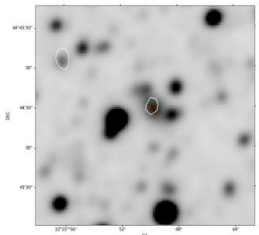

J234136+321424

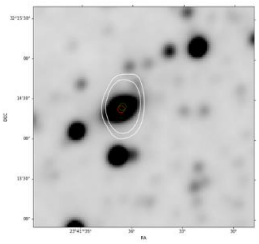

J131047+29424

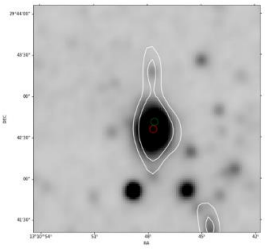

J134248+301226

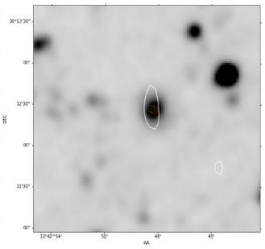

J130422+284838

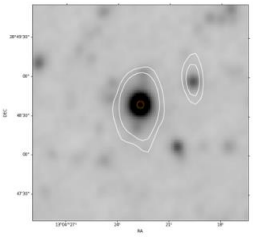

J130622+293925

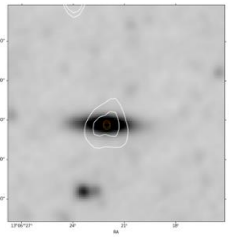

J130855+280131

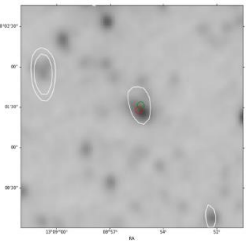

J140155+322730

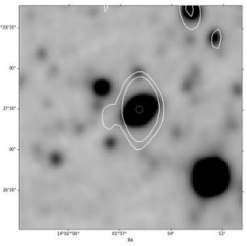

J130225.64+285129.0

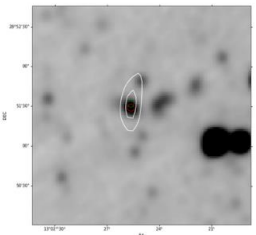

J130545.25+285212.1

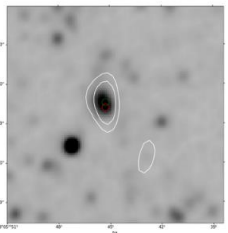

J130832.56+304452.5

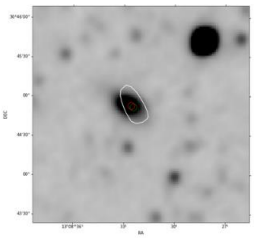

J222741+352423

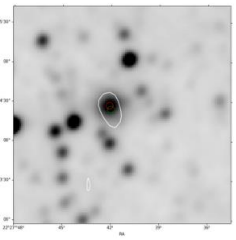

J140348+333410

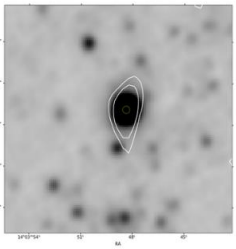

J014331+325250

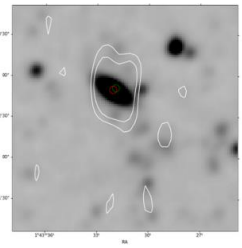

J015521.18+313733.6

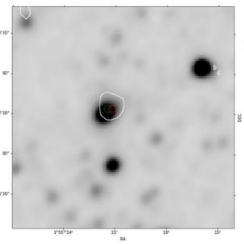

J222053+331741

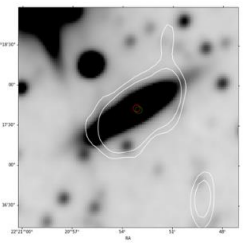

J131825+312807

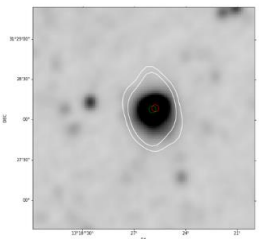

J131650+313749

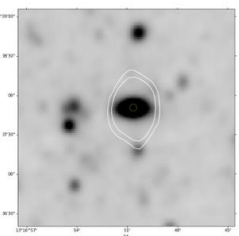

J233543.63+322304.5

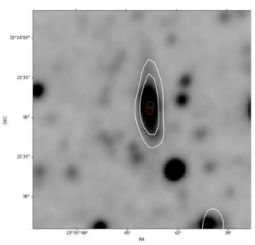

J014104.43+315247.8

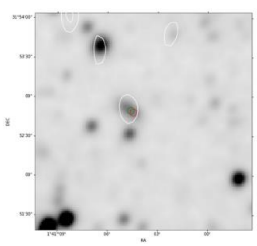

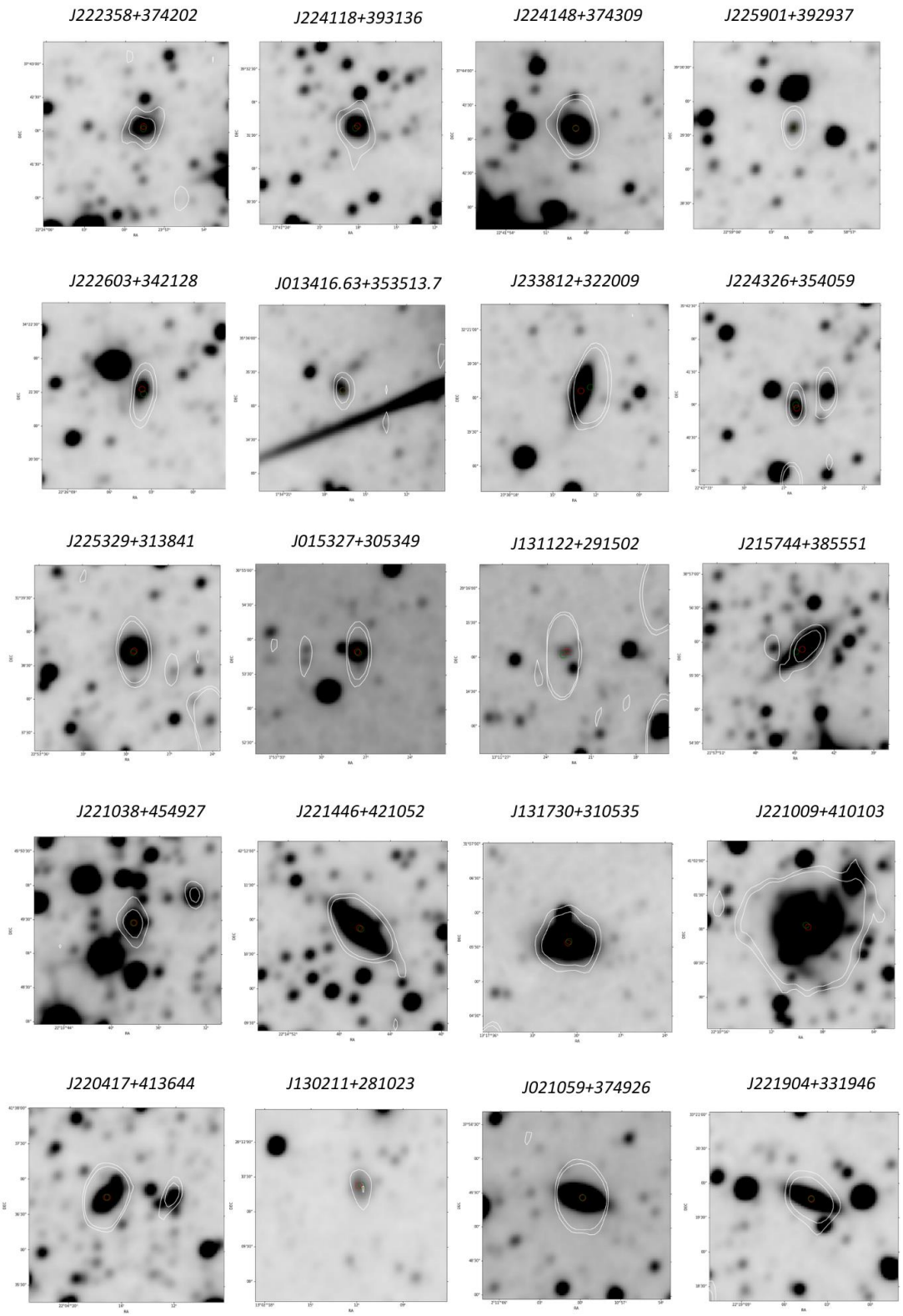
J222358+374202
J224118+393136
J224148+374309
J225901+392937
J222603+342128
J013416.63+353513.7
J233812+322009
J224326+354059
J225329+313841
J015327+305349
J131122+291502
J215744+385551
J221038+454927
J221446+421052
J131730+310535
J221009+410103
J220417+413644
J130211+281023
J021059+374926
J221904+331946

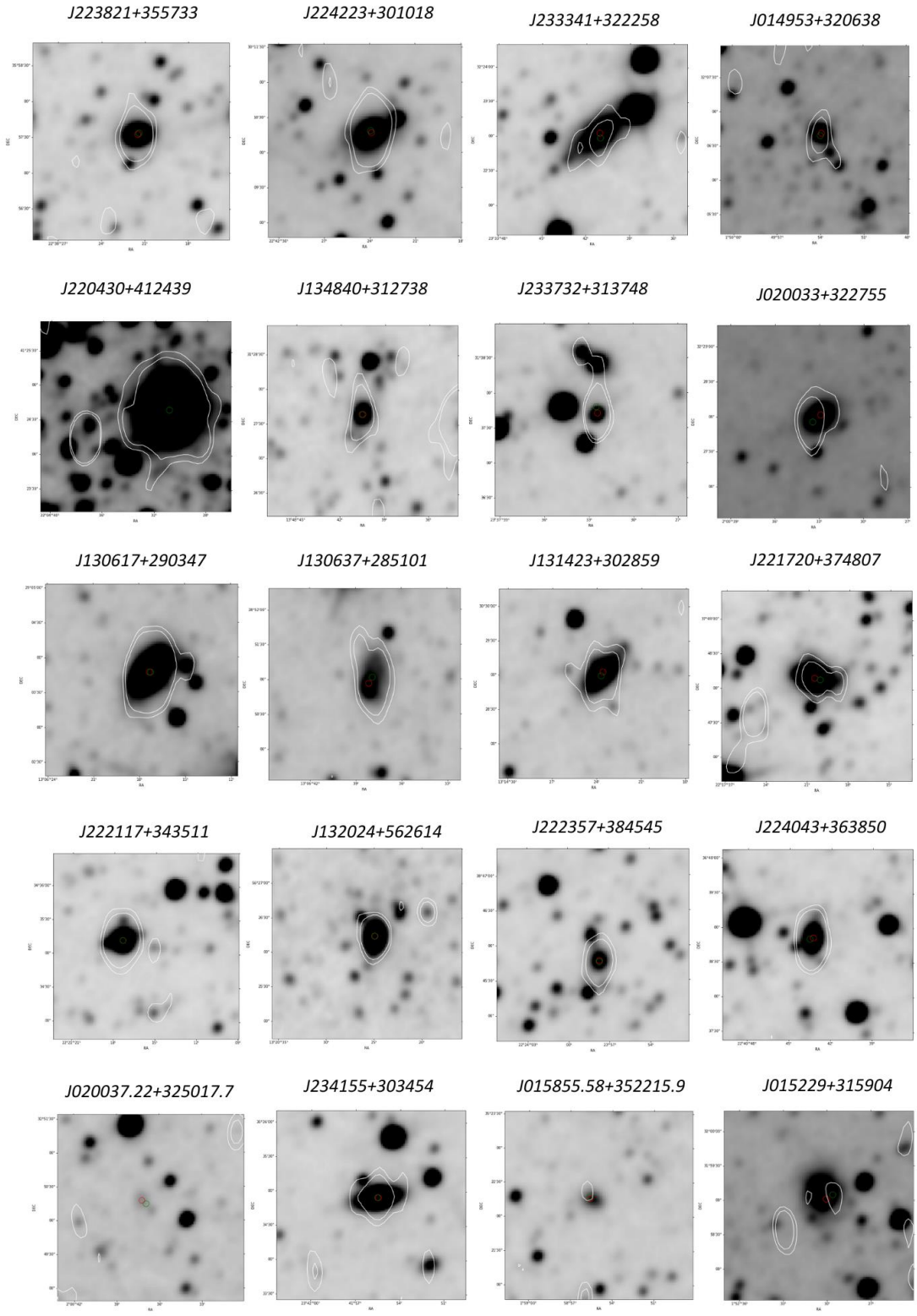
J223821+355733
J224223+301018
J233341+322258
J014953+320638
J220430+412439
J134840+312738
J233732+313748
J020033+322755
J130617+290347
J130637+285101
J131423+302859
J221720+374807
J222117+343511
J132024+562614
J222357+384545
J224043+363850
J020037.22+325017.7
J234155+303454
J015855.58+352215.9
J015229+315904

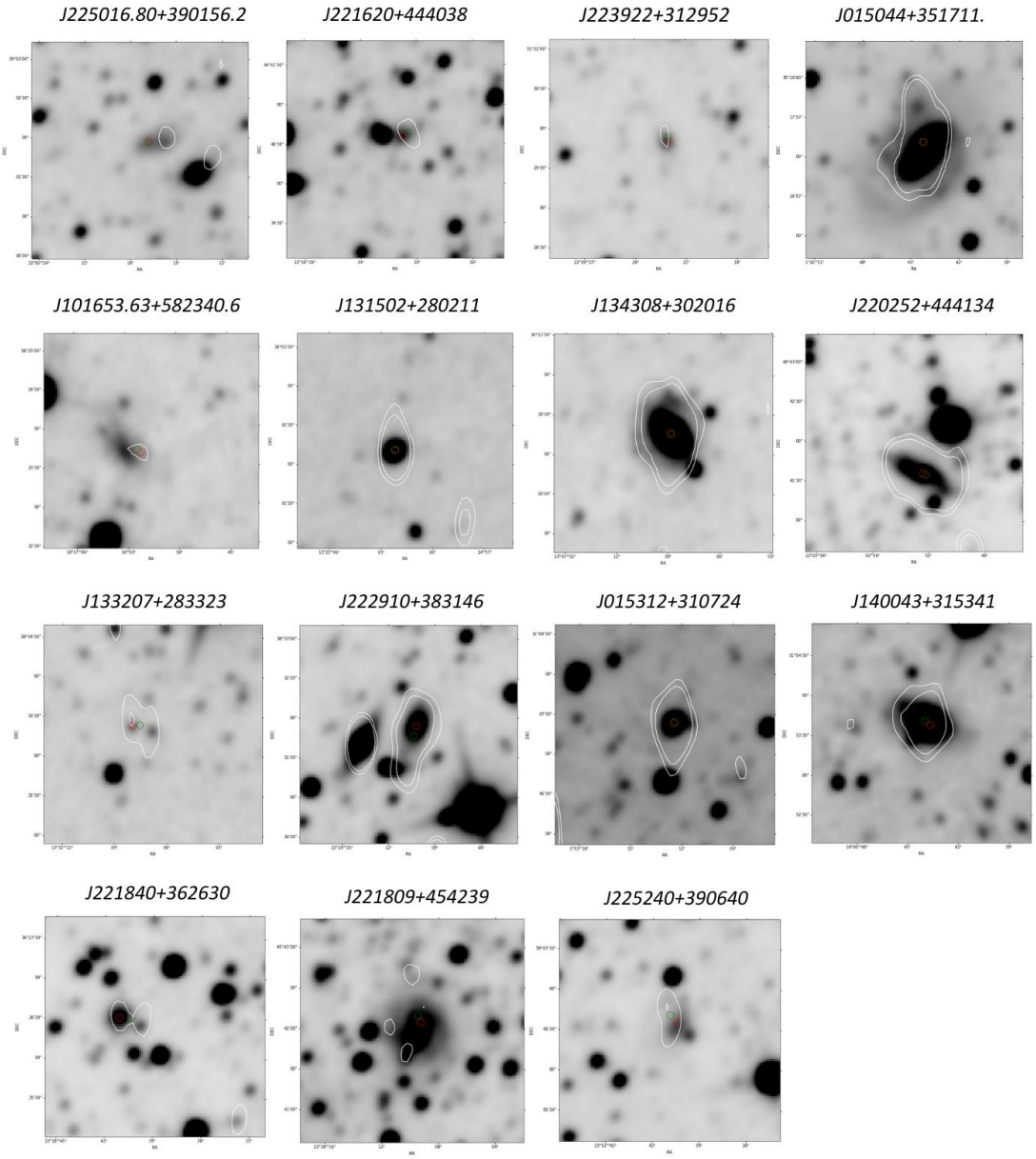
J225016.80+390156.2
J221620+444038
J223922+312952
J015044+351711.
J101653.63+582340.6
J131502+280211
J134308+302016
J220252+444134
J133207+283323
J222910+383146
J015312+310724
J140043+315341
J221840+362630
J221809+454239
J225240+390640

WISE CONTAMINATION

J225623+342726

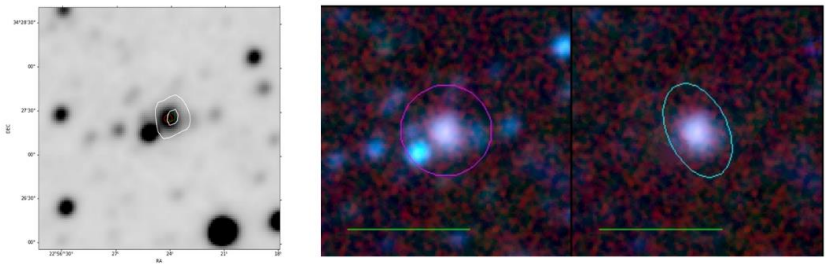

J014627+345536

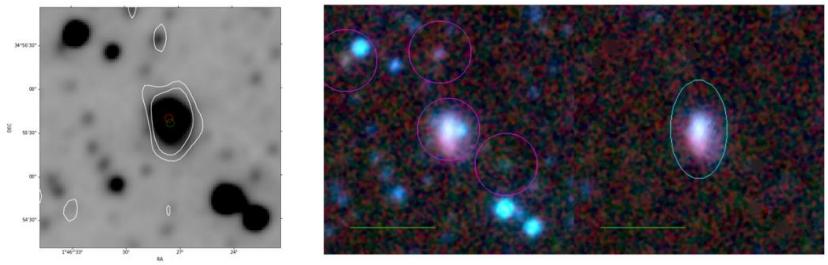

J015350+363352

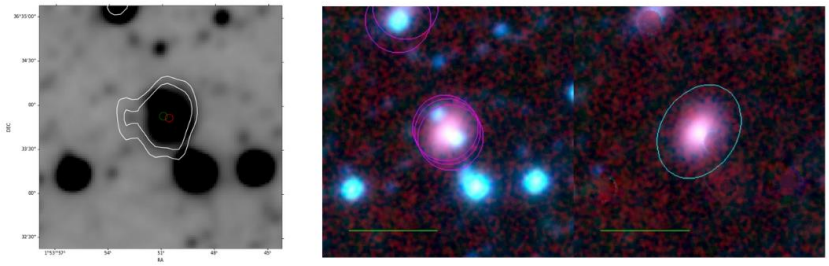

J102524+553126

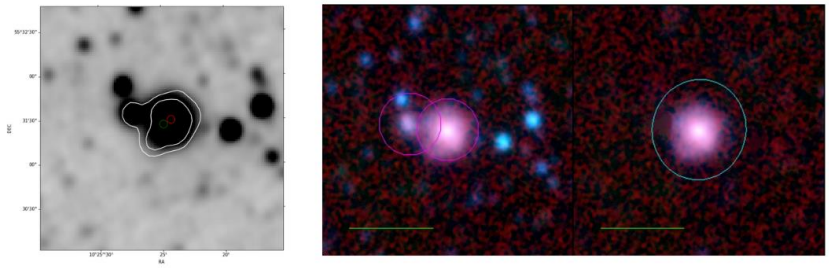

J234411+314559

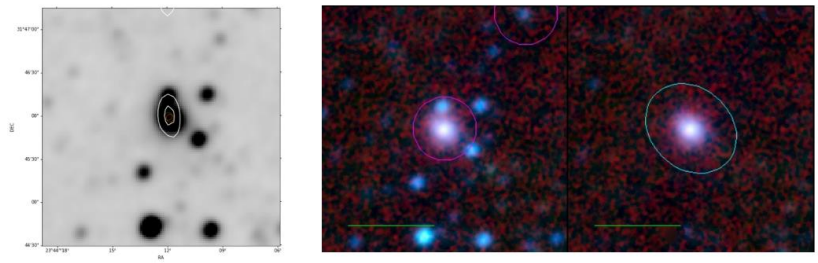

J220733+415016

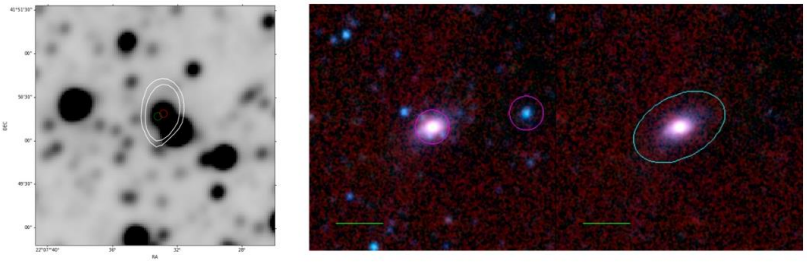

J015623+371258

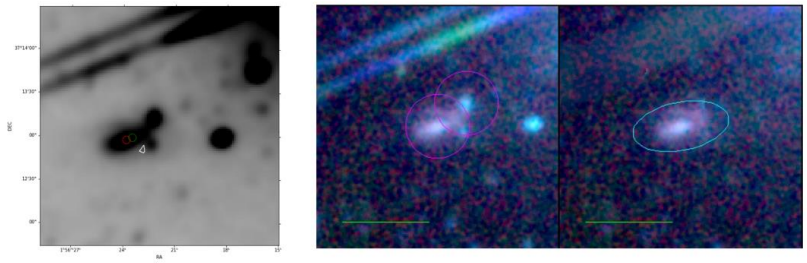

J222553+401849

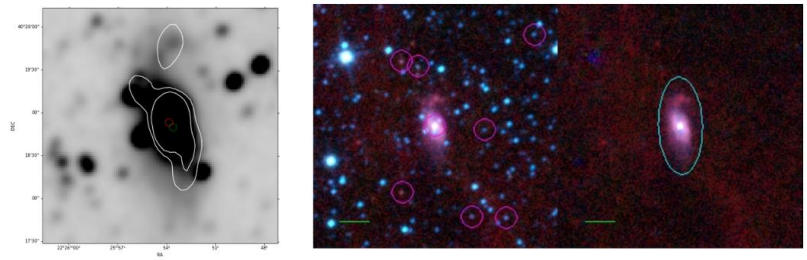

J230748+301901

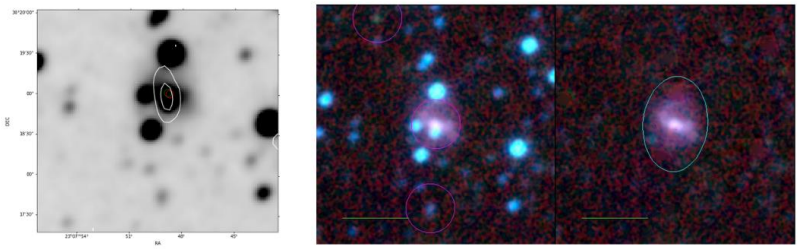

J230546+383848

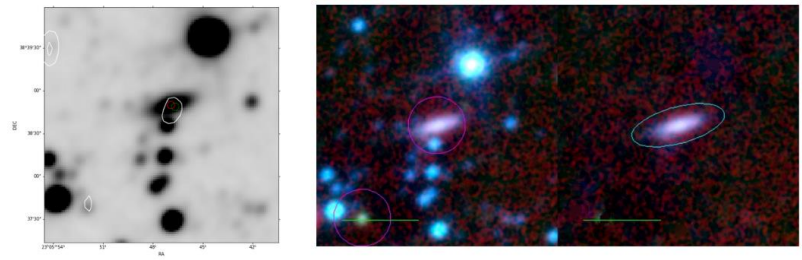

J220506+452955

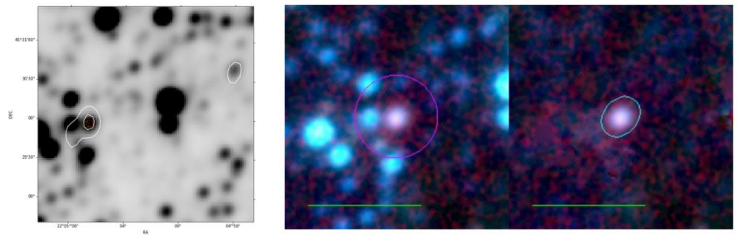

J221920+434859

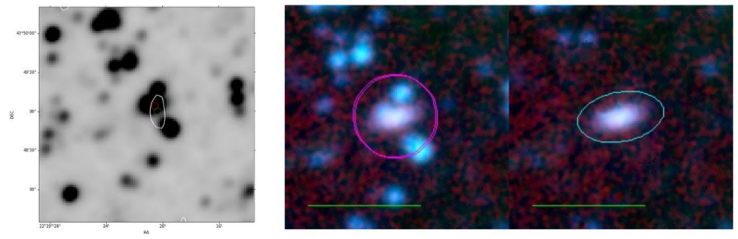

J223257+352702

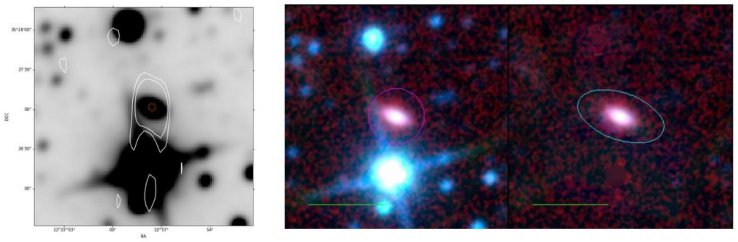

J223653+353013

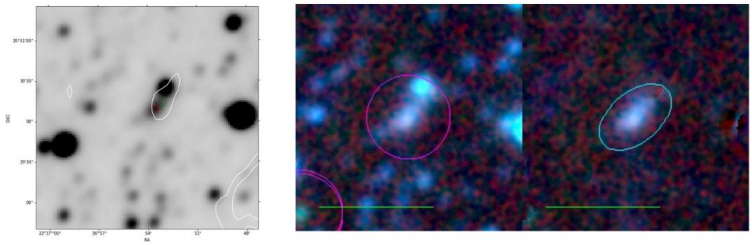

J225452+324734

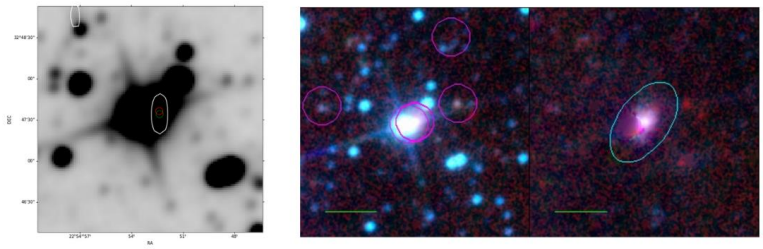

J131244+314829

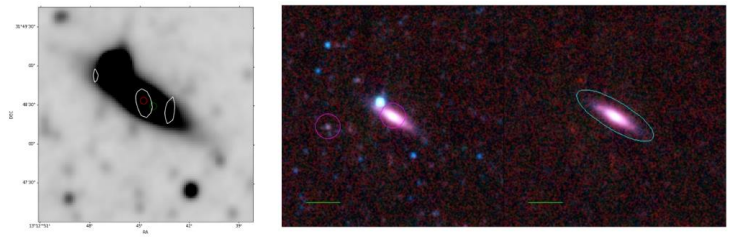

J162436+530718

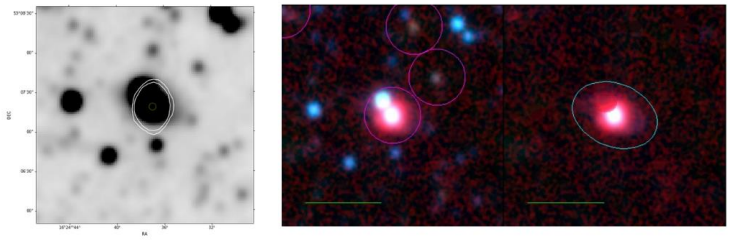

J220015+385932

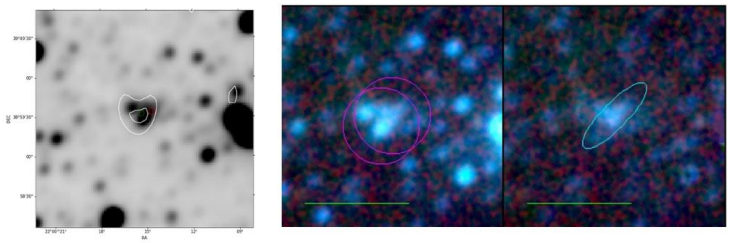

J220808+453416

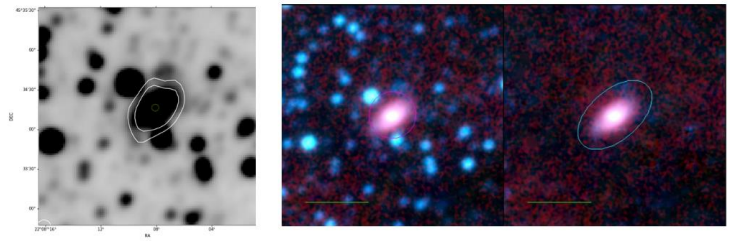

J014811+352359

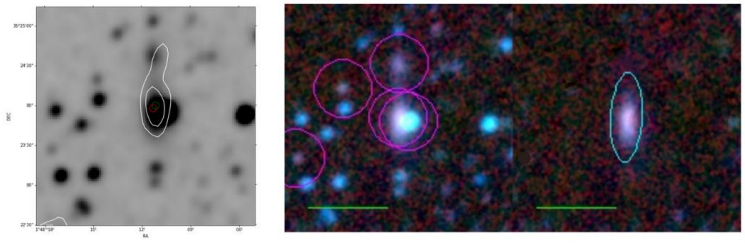

J224716+385823

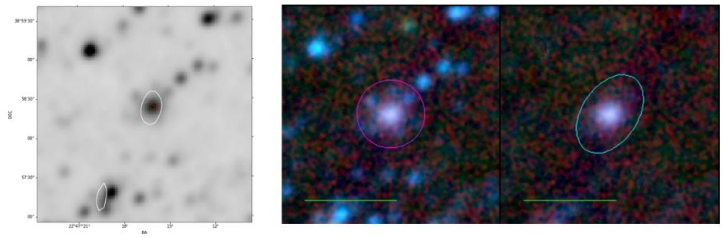

J224325+374104

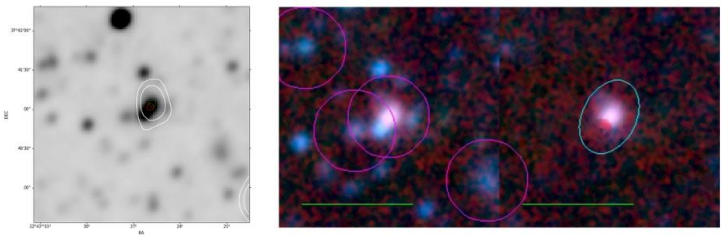

J220537+445018

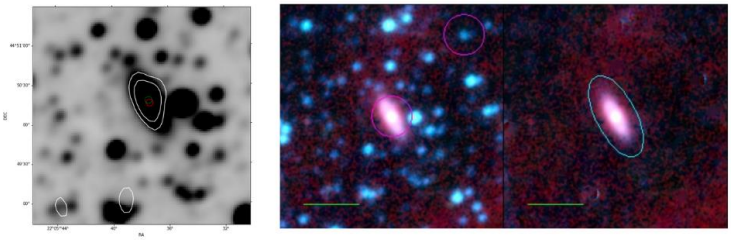

J140016+310300

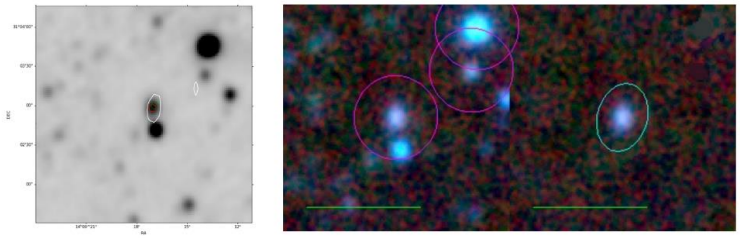

J020036+325014

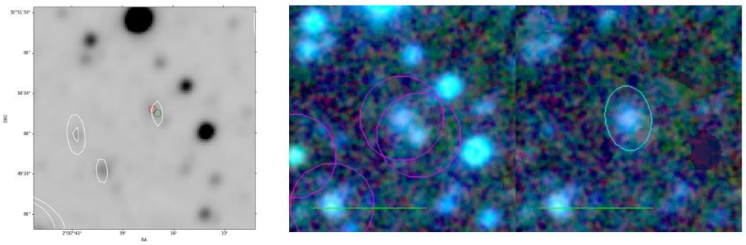

J220854+445729

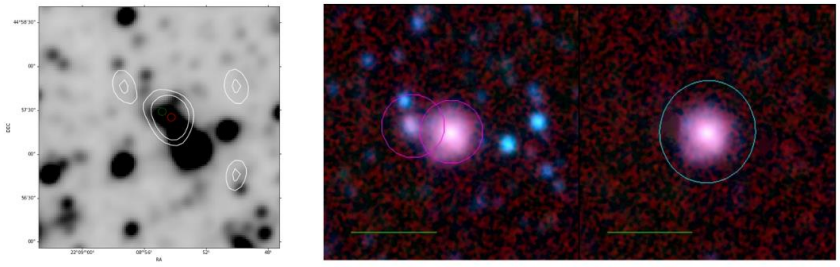

J131939+301523

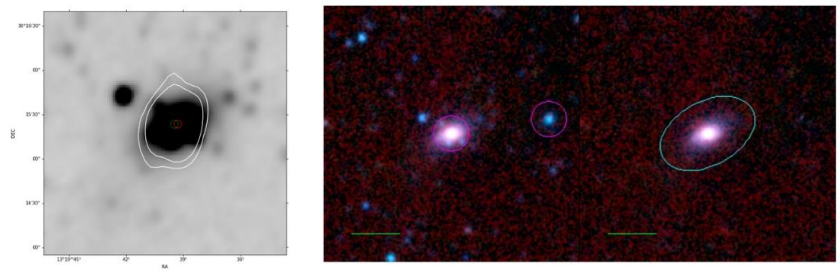

J162323+530501

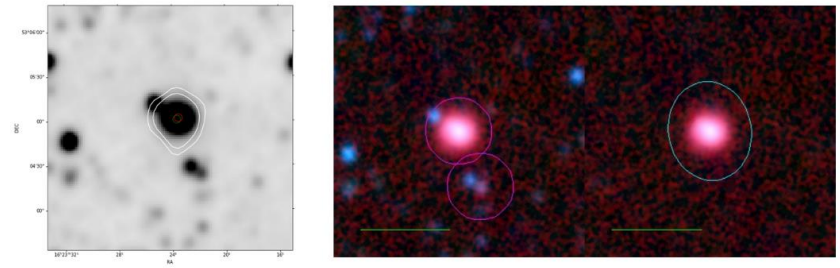

J014028+343732

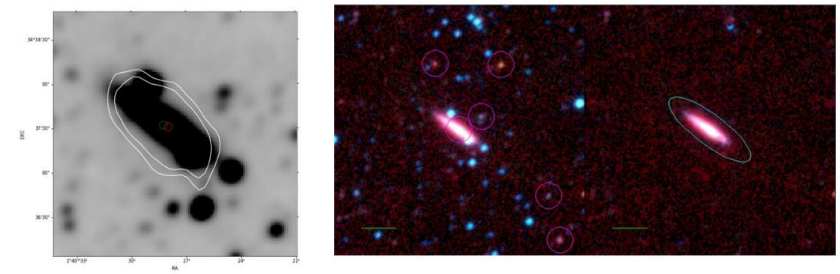

J222218+444251

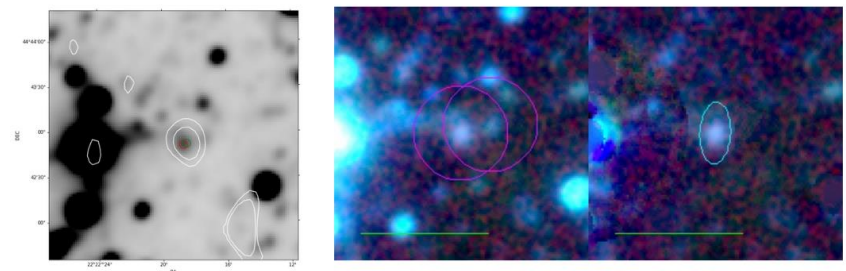

J220359+455013

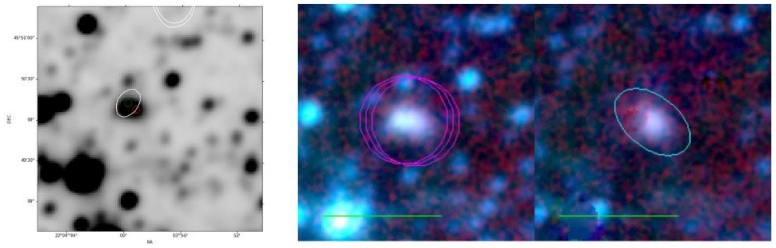

J220921+445824

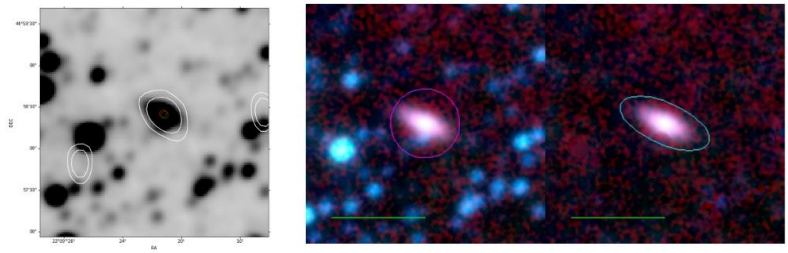

J233917.93+312715.3

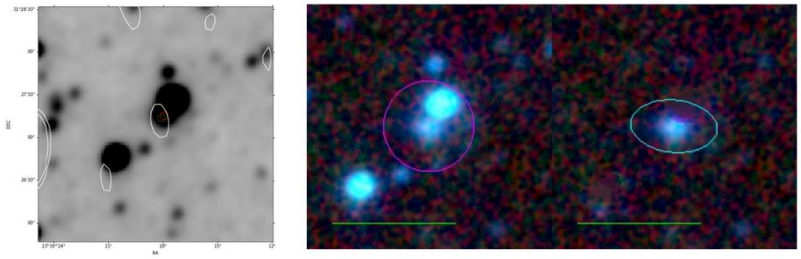

J224226+361333

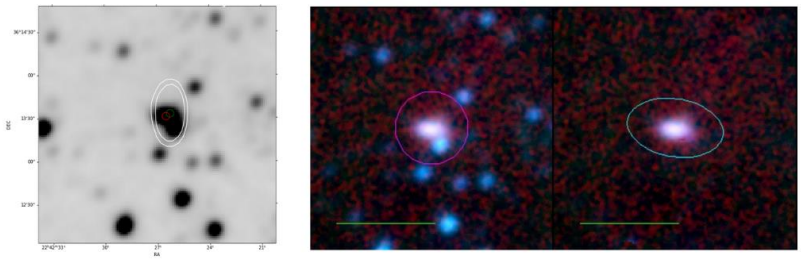

J131547+315047

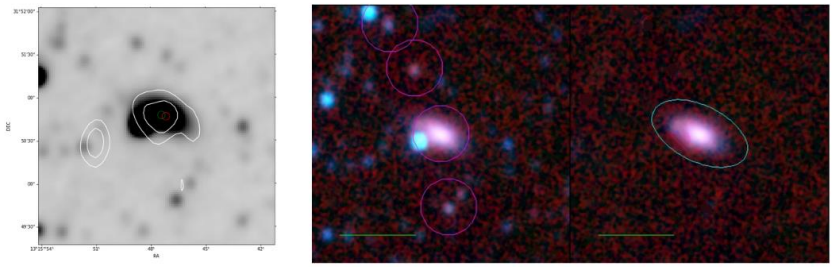

J101156.61+584403.2

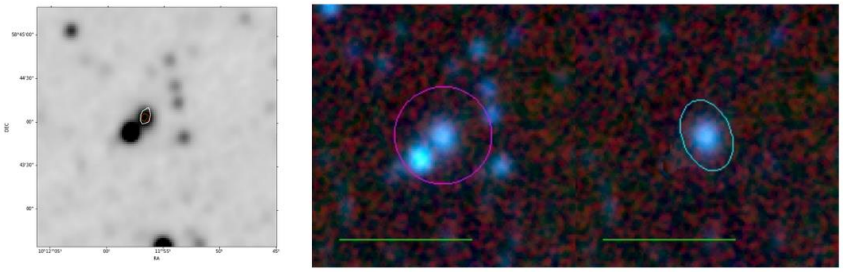

J015958+363526

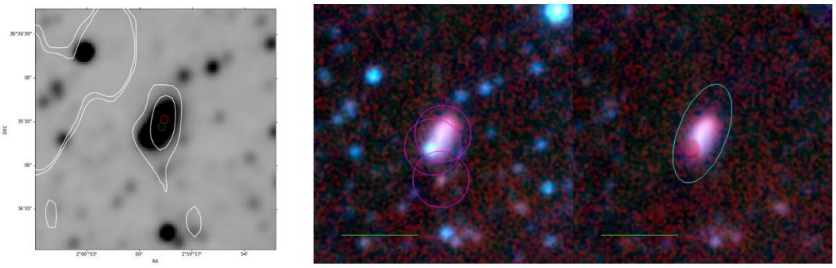

J220812+411616

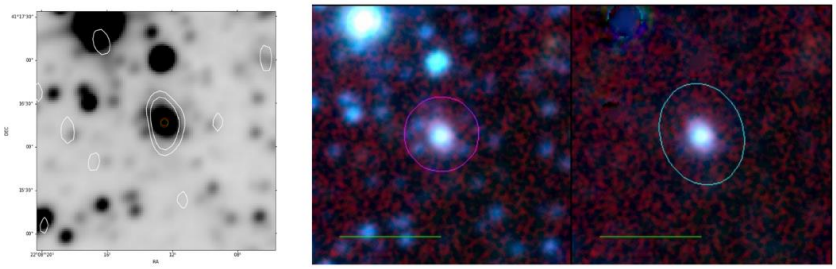

J220952.31+412755.0

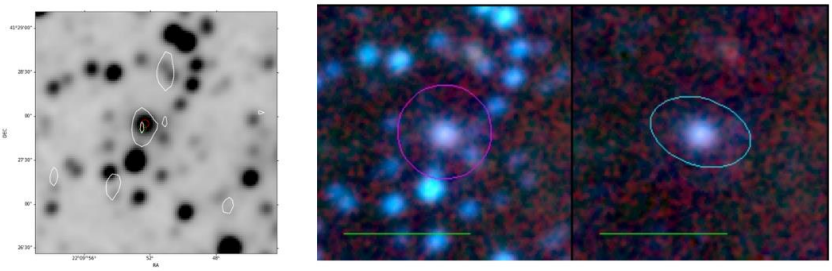

J221814+434912

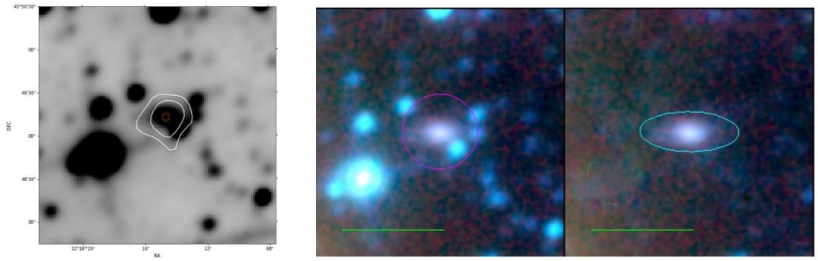

J222150+425702

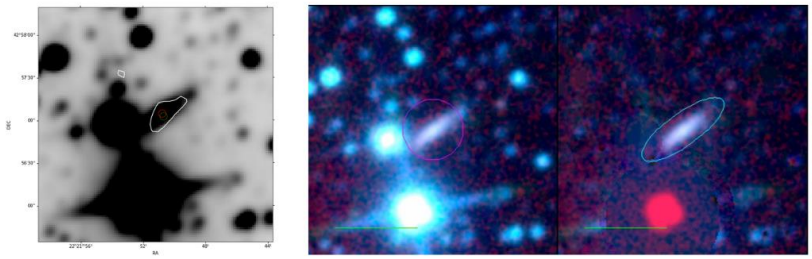

J222909+364725

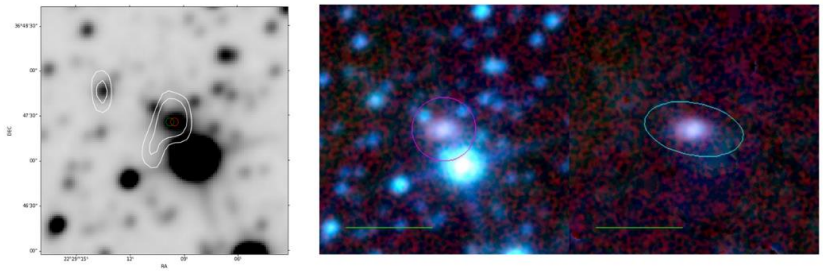

J222952+364308

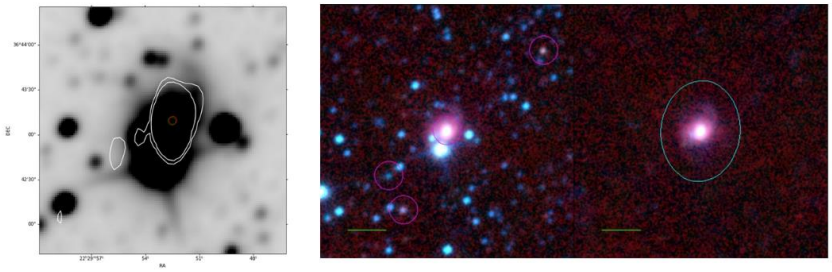

J224945+412159

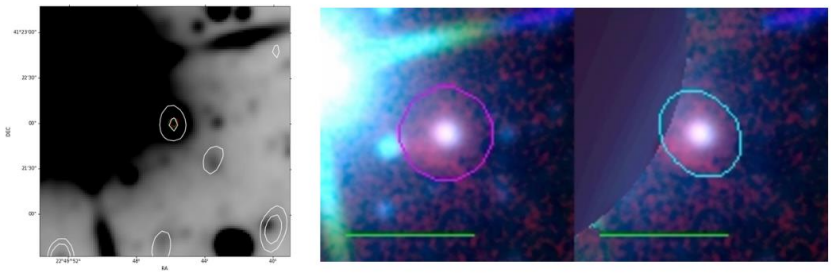

J125426+595805

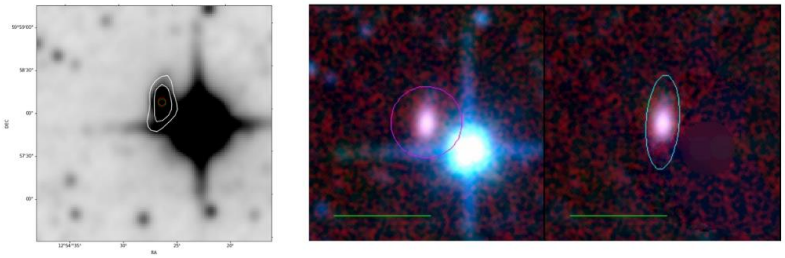

J015353+363513

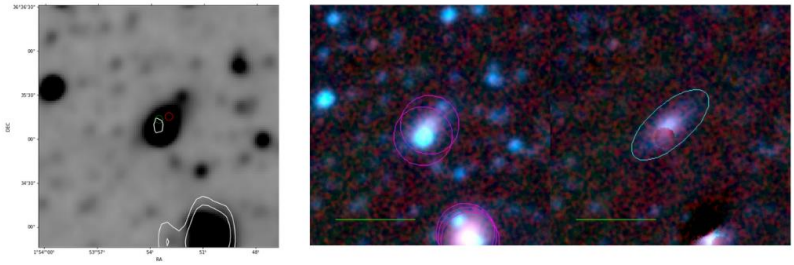

J143538+554619

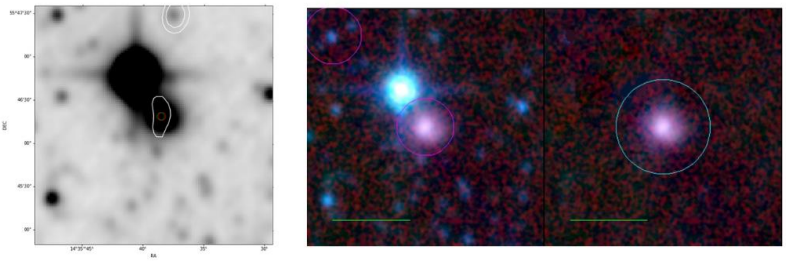

J220703+455605

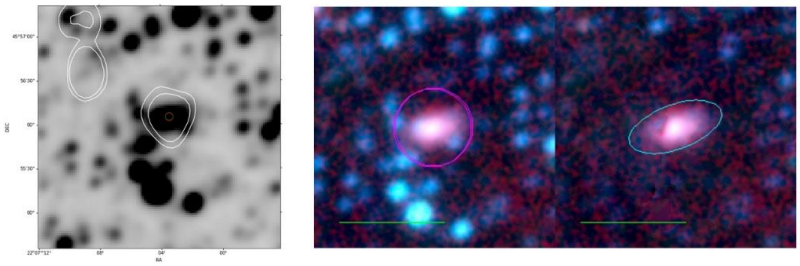

J220854+402055

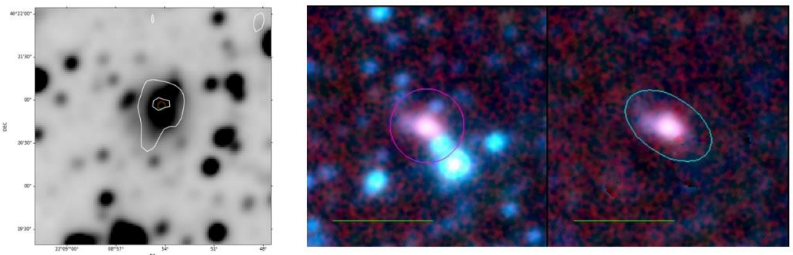

J015414+320707

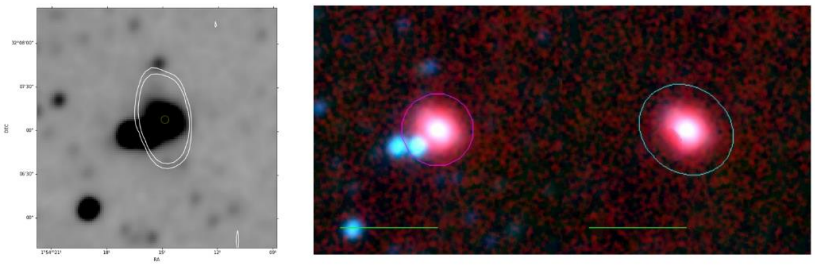

J104454+515857

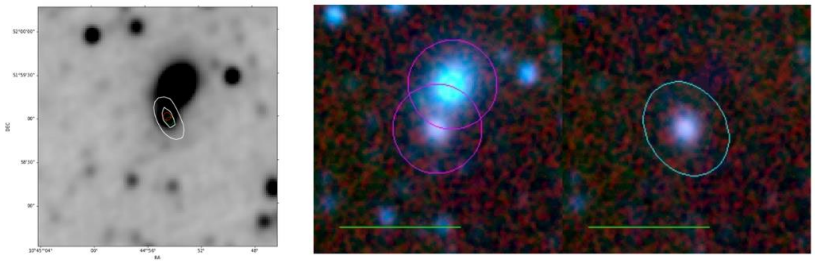

BAD MATCH

J132712+552915

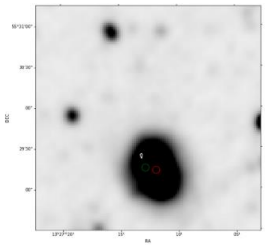

J142408+545156

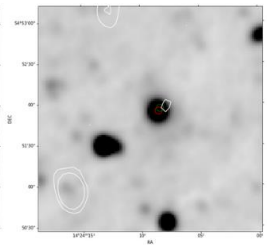

J221534+462829

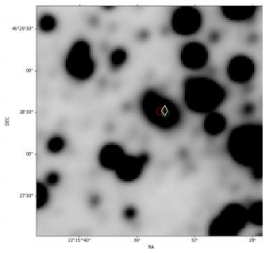

J231150+310116

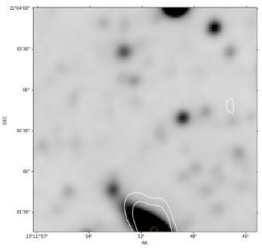

J021002.41+370212.7

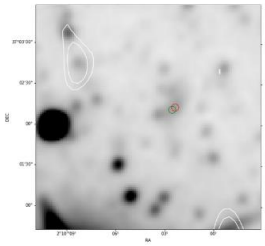

J224731+403402